

2

The atmosphere of the Earth

2.1 NOMENCLATURE

The atmosphere of the Earth is an ocean of gas encircling the globe. It stretches out far from the surface; how far out is a question of definition.

In [Figure 2.1](#) we have illustrated schematically the variation of some characteristic parameters up to an altitude of 450 km. There are rather strong variations in the upper atmosphere above 100 km during a solar cycle, and this is illustrated in the figure by curves representing average solar maximum and minimum conditions. The cross-hatched areas between these curves illustrate the variability of the parameters. The number density (n) of the atmosphere decreases monotonically with height from 10^{25} m^{-3} at ground level to 10^{14} m^{-3} at 400 km. The atomic mass number is constant and close to 30 at the ground and up to about 100 km; above that region it decreases gradually toward 15 at 400 km. This corresponds to an air density of 1.2 kg/m^3 at ground level decreasing to about $3.4 \times 10^{-6} \text{ kg/m}^3$ at 90 km, $2.4 \times 10^{-8} \text{ kg/m}^3$ at 120 km, and $2.8 \times 10^{-10} \text{ kg/m}^3$ at 200 km, respectively. According to variations in its composition the atmosphere is divided into two main regions, the *homosphere* and the *heterosphere*, indicating that below 100 km the gas constituents are fully mixed into a homogeneous gas. Above this height, however, the different constituents behave independently, and the atmosphere is heterogeneous.

The temperature (T) of the atmosphere has a more complicated behavior with height. It starts out by decreasing in the *troposphere* from about 290 K at the ground and reaching a minimum close at 215 K at 1,520 km, called the *tropopause*.

Above the tropopause is the *stratosphere*, and here the temperature increases up to a maximum of close to 280 K, called the *stratopause*, usually situated close to 50 km. Above the stratopause the temperature decreases again in the *mesosphere* and reaches the lowest temperature in the atmosphere in the *mesopause*, usually situated at about 70–90 km. The temperature in the mesopause may be as

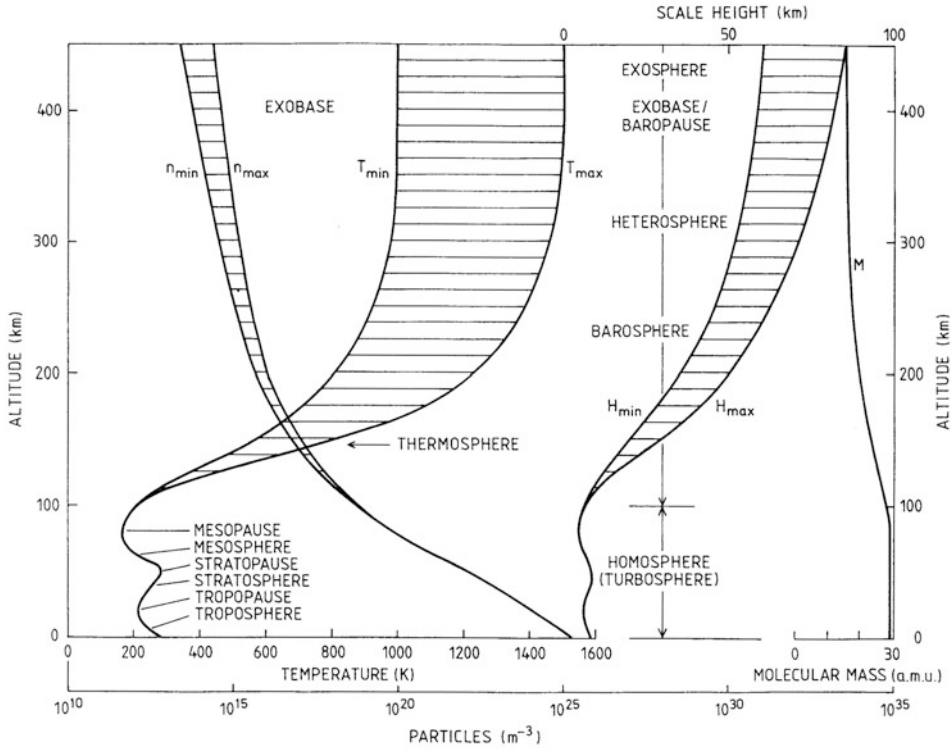


Figure 2.1. Model height profiles of the temperature T , density n , molecular mass M , and scale height H distributions in the Earth's atmosphere below 450 km. The different regions are also indicated by their characteristic names according to temperature or composition. Variability in the different parameters with respect to solar activity is indicated by the hatched areas.

low as 160 K or even lower at occasions. As a curiosity, however, the mesopause temperature in polar regions is higher in winter than in summer.

Above the mesopause the temperature increases dramatically in the thermosphere where temperatures of more than 1,000 K can be found above the *exobase* indicated in Figure 2.1 at 400 km. Above this region the temperature is fairly constant by height, but may vary considerably by time.

The nomenclature used for characterizing different areas in the atmosphere refers to either temperature, composition, or dynamics. At the ground we find that the atmosphere is composed of close to 80% N_2 and 20% O_2 , while the contribution from other gases is less than 1%. This mixture holds all the way up to about 100 km. The region below 100 km is therefore called the *homosphere* or the *turbosphere*. The latter reflects the fact that turbulence causes the mixture. Above 100 km, molecules start to dissociate and become more independent of each other; they are more heterogeneous. This region is therefore called the *heterosphere* or the *barosphere*; the latter reflecting the fact that the different species have different scale heights or barometric heights.

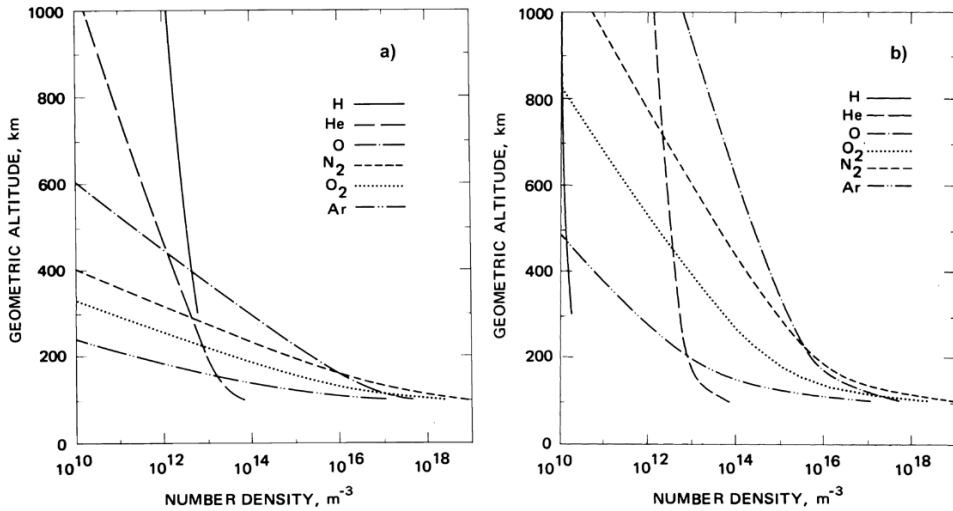


Figure 2.2. Composition changes in the atmosphere with respect to (a) solar minimum and (b) solar maximum conditions showing the dominance of heavier constituents at larger altitudes during solar maximum. (From U.S. Standard Atmosphere, 1976.)

In [Figure 2.2](#) we show a more detailed presentation of the altitude profiles of different atmospheric species between 1,000 km and the ground under solar minimum and maximum conditions. While atomic oxygen dominates the upper atmosphere above 250 km under solar maximum conditions, hydrogen is more dominant above 400 km under solar minimum conditions. Below 200 km, however, molecular oxygen and nitrogen together with argon are the dominant species independent of solar activity.

Due to the composition at ground level (80% N_2 and 20% O_2) the average molecular mass will be 28.8 a.m.u. Since molecules start to dissociate above about 100 km and nitrogen molecules dissociate faster than oxygen molecules, the molecular weight will decrease and oxygen atoms will be the dominant species from 400 km to above 1,000 km, at least during solar cycle maximum (see [Figure 2.2](#) for references).

At 600 km where we might have 84% O and 16% He, the molecular mass is 14 a.m.u. While the number density at the ground is about $2.5 \times 10^{25} \text{ m}^{-3}$, it is about 10^{19} m^{-3} at 100 km, and at 200 km it has been reduced to about 10^{16} m^{-3} . The density therefore has decreased by more than 10^9 from the ground up to typical rocket trajectories.

2.2 TEMPERATURE STRUCTURE OF THE ATMOSPHERE

The temperature in the atmosphere decreases quite monotonically up to the tropopause. This is due to the fact that infrared radiation from the ground, which

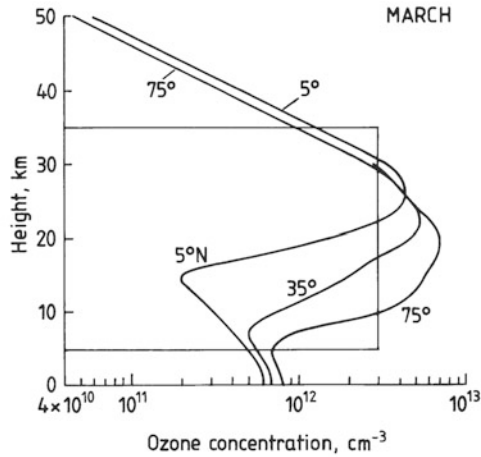


Figure 2.3. Ozone density profiles in the atmosphere at different latitudes in the northern hemisphere. The concentration is given in molecules per cm^3 . (After Shimazaki, 1987.)

is absorbed in the atmosphere, is rather constant because the surface temperature of the globe is constant, and therefore the heat expands out in the atmosphere in radial directions. The heat will then be distributed into larger and larger volumes and therefore the temperature must decrease.

Due to the ozone layer situated between 5 and 40 km above the ground depending on latitude (Figure 2.3) which absorbs a large portion of the solar radiation between 200 and 300 nm, the atmosphere becomes heated in the stratosphere and the temperature increases. Above the stratopause, however, the heat balance results in excess outward radiation again, and the temperature decreases rapidly in the mesosphere until the sharp minimum occurs at the mesopause.

By observing the ozone density profile at different latitudes, however, the peak altitude is found to decrease and the peak magnitude to increase with increasing latitude. More ozone is therefore present at lower altitudes (<25 km) in the polar region (Figure 2.3).

This is even more clearly brought out in Figure 2.4 where the latitudinal average of the ozone content at different altitudes below 50 km is presented versus the latitude for the average February month. The winter pole has rather high ozone content at low altitudes (<20 km) while the ozone density above the equator is much smaller and maximizes above 20 km. This latter effect cannot be explained by the simple photochemical equilibrium models of the atmosphere since from these we would expect the ozone content to be high at lower heights in the equatorial region where the solar radiation and the radiative dissociation of O_2 is highest. Transport processes must therefore be of fundamental importance for global ozone distribution.

In Figure 2.5 the latitudinal distribution of total ozone content for different seasons of the year is presented. Again there are clear maxima above the polar regions, but it is seen that these maxima occur in spring. The maximum in the

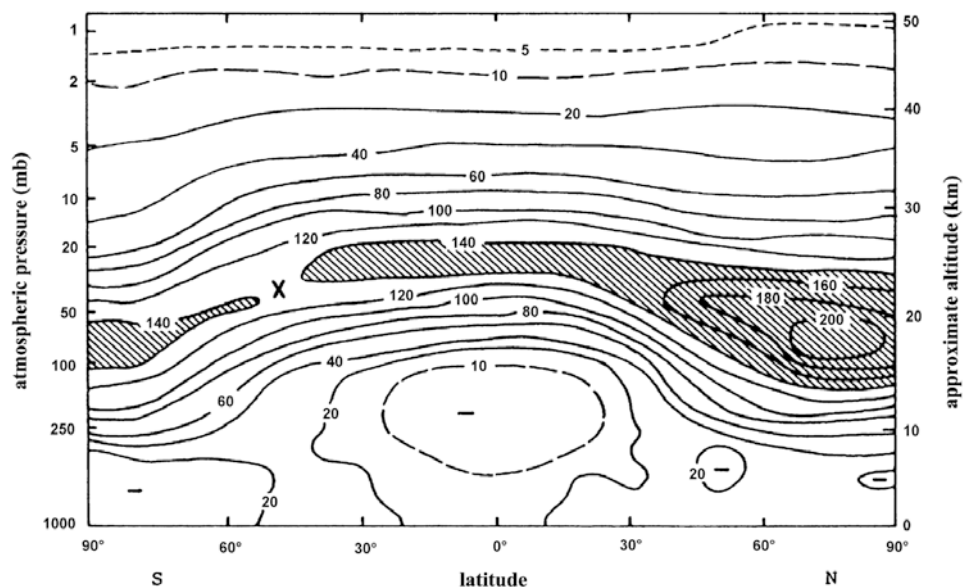


Figure 2.4. Latitudinally averaged ozone distribution for February shown as a function of height and latitude. A strong maximum is observed below 20 km in the Arctic region. (From Dütsch, 1978.)

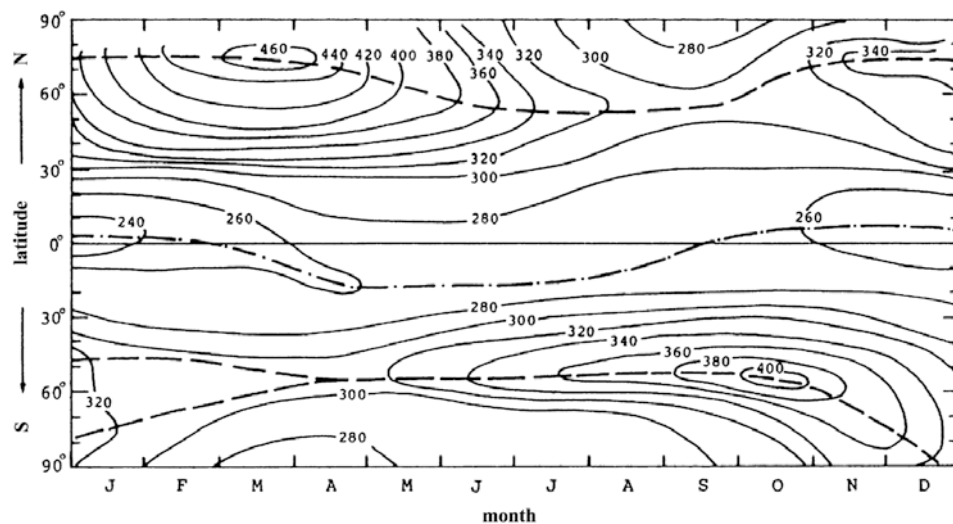


Figure 2.5. Latitudinal and seasonal variation of the total ozone content. The labels added to the isolines are given in Dobson units. (From London, 1985.)

northern hemisphere in March is about 15% higher than the corresponding maximum in the southern hemisphere in October.

In the northern hemisphere the amplitudes of seasonal variation are also larger, varying from a maximum of close to 460 Dobson units in April at times to about 280 Dobson units in November. That is a variation of more than 20% around the mean value.

The total ozone content in a vertical column above a ground-based observer has been measured for more than 50 years at different places on Earth.

The term “total ozone”, sometimes referred to as total layer thickness, thus represents the height integral of the column density and is often abbreviated as atm-cm or cm (STP). This corresponds to the thickness of the layer if the pressure and density were reduced to standard atmospheric values throughout the layer. The Dobson unit is derived in a similar manner and abbreviated as m-atm-cm which equals 10^{-3} atm-cm. Therefore, 300 Dobson units represent an ozone content which, when reduced to standard temperature and pressure throughout the layer, would correspond to a column of 3 mm.

One of the early findings in the research of ozone was the smaller amount of ozone in the Antarctic spring than in the Arctic spring. Another early result of such measurements was the occasional decrease observed in total ozone during the early springtime.

As is well known, the ozone layer shields the Earth from UV radiation which can be a health hazard to some people. The shielding, however, is most effective in the polar region where the ozone layer is at its thickest and the Sun has a large angle to the zenith, while the layer is more shallow at lower latitudes where the Sun is close to overhead. This is illustrated in [Figure 2.6](#).

For a station at 70° latitude, for example, the Sun can never make an angle α with the zenith less than 46.5° . Therefore, the distance that the solar UV ray must pass through the ozone layer will be ([Figure 2.7](#))

$$l = \frac{h}{\cos \alpha}$$

if h is the thickness of the layer. In the tropics where the Sun can be at zenith and $\alpha = 0$, the ray path through the layer is equal to the layer thickness. In order for the UV intensity observed at 70° latitude to be equal to the intensity observed at the equator the layer thickness at 70° is to a first approximation given by:

$$h' = h_e \cos \alpha$$

Since the present thickness of the ozone layer at high latitudes is about $1.5h_e$ we notice that the layer thickness must be reduced to about half its present value:

$$\frac{h'}{h} = \frac{h_e}{1.5h_e} \cos 46.5 \approx 0.5$$

Above the mesopause solar radiation in the UV band is strongly absorbed owing to dissociation of molecules such as O_2 , N_2 , and NO and ionization of

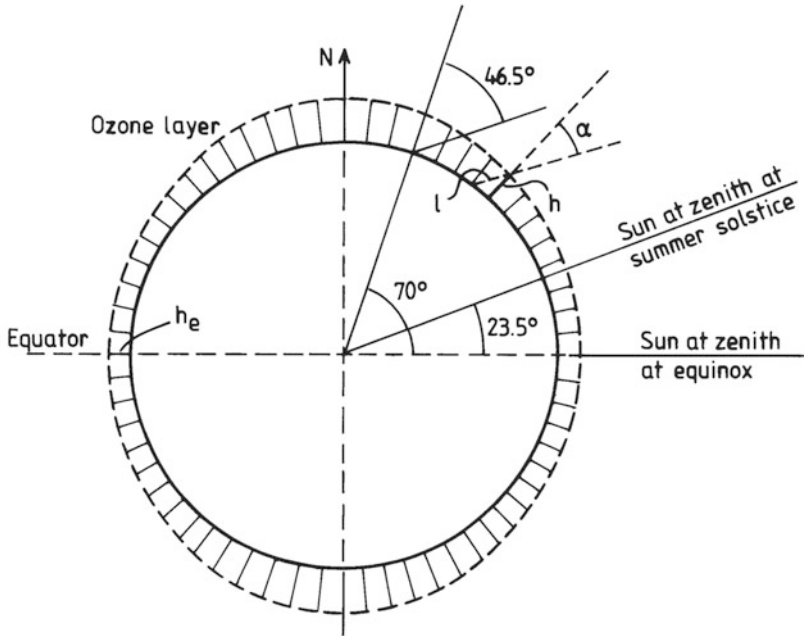


Figure 2.6. A schematic illustration of the global ozone distribution showing a thinning of the layer at lower latitudes where also solar irradiation can have a vertical impact on the atmosphere. The height of the maximum in the layer, however, is larger at equatorial regions than at the poles.

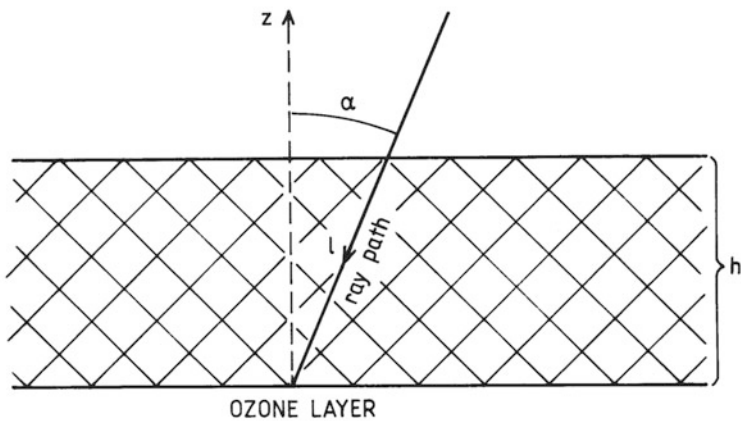


Figure 2.7. Illustration of variation in the length of the ray path through the ozone layer with a varying solar zenith angle.

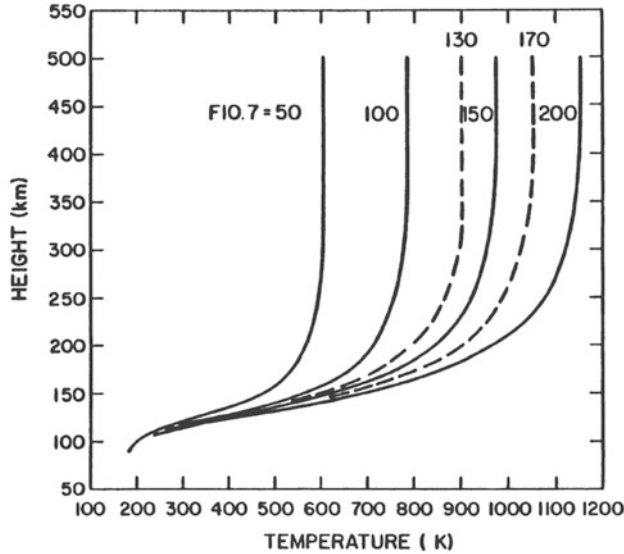


Figure 2.8. Variability in the thermospheric temperature for different values of the solar radio flux index ($F_{10.7}$) in units of $10^{-22} \text{ W m}^{-2} \text{ Hz}^{-1}$ reduced to 1 AU. Under average solar minimum and maximum conditions the $F_{10.7}$ index is 50 and 200, respectively. (From Roble, 1987.)

atomic oxygen and other molecules and atoms. This leads to a new temperature increase which is particularly strong up to about 400 km.

The very strong absorption of UV radiation in the thermosphere, however, is accompanied by strong variability in the temperature of this region as illustrated in [Figure 2.1](#). This is because solar UV radiation itself is so variable. As the temperature above 400–600 km appears fairly constant with height as a function of altitude, it is often referred to as the exospheric temperature (T_{∞}). [Figure 2.8](#), which is an alternative presentation of [Figure 2.1](#) above 100 km, shows the range of variability in thermospheric temperature at different altitudes in the course of a solar cycle due to variations in the exospheric temperature. The intensity index of solar radio emission at $F_{10.7}$ is used as a reference parameter to the solar cycle. The value 50 represents solar minimum conditions while the value 200 represents solar maximum conditions.

The exospheric temperature can change by 600 K or more during a solar cycle according to similar model calculations (as presented in [Figure 2.8](#)).

The thermospheric temperature, however, is not constant all over the globe and exhibits a seasonal variation. The thermospheric temperature at 300 km as a function of latitude for solstice and equinox conditions is presented in [Figure 2.9](#). Also shown in [Figure 2.9](#) is the mean molecular mass (a.m.u.) for the corresponding conditions. At solstice especially, latitudinal variations are as large as the temperature changes from close to 1,400 K at the summer pole to slightly above 900 K at the winter pole, and the molecular mass changes from 21 a.m.u. to 17 a.m.u. in the same region.

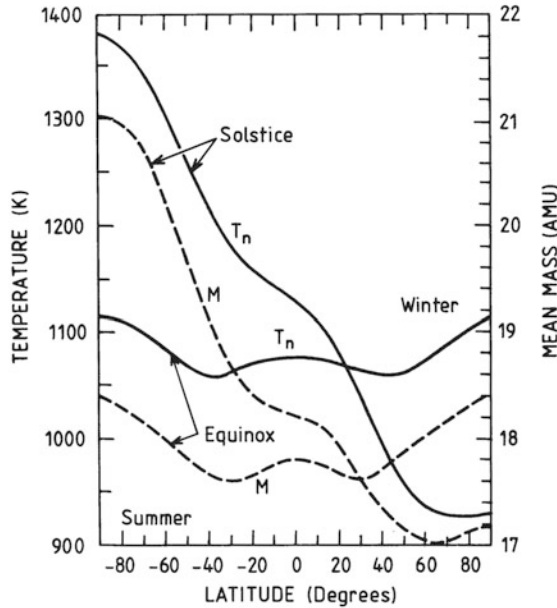


Figure 2.9. Latitudinal distribution of the neutral temperature T_n and mean molecular mass M at 300 km under equinox and solstice conditions. (After Roble, 1987.)

The consequence of this is that heavier molecules are brought up to higher altitudes from below in the summer hemisphere and downward in the winter hemisphere (Figure 2.10). The summer thermosphere at 300 km and above is therefore dominated by N_2 molecules, while the winter thermosphere in the same height region has a large contribution of helium atoms.

The thermospheric temperature also responds to solar variations on a shorter time scale than solar cycles or seasonal periods. Figure 2.11 presents a comparison of variations in exospheric temperature T_∞ , atmospheric mass density ρ , solar radio emission flux S ($= F_{10.7}$), and a geomagnetic index Ap . The latter represents variations in the Earth's magnetic field, presumably due to ionospheric currents.

The 27-day period in solar radio emission, S ($F_{10.7}$), is clearly reflected in T_∞ as well as ρ , as if the atmosphere is expanding and contracting as the solar flux increases and decreases.

2.3 ATMOSPHERIC DRAG ON SATELLITES

Figure 2.12 gives a schematic presentation of the variability of atmospheric density between 100 and 1,000 km under solar maximum and minimum conditions as well as under extreme solar maximum daytime conditions. Density variations of two orders of magnitude can in fact take place during a solar cycle above 400 km altitude.

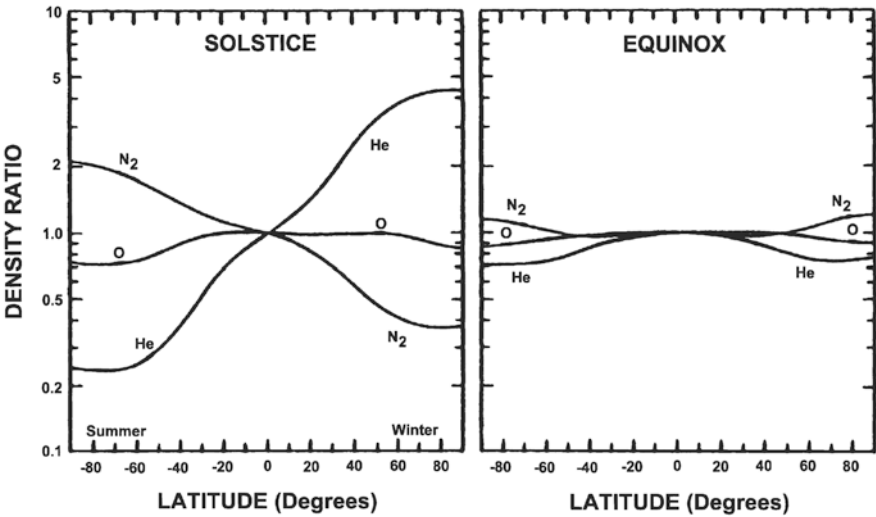


Figure 2.10. The latitudinal distribution of molecular nitrogen (N_2), atomic oxygen (O_2), and helium (He) under solstice and equinox conditions. (From Roble, 1987.)

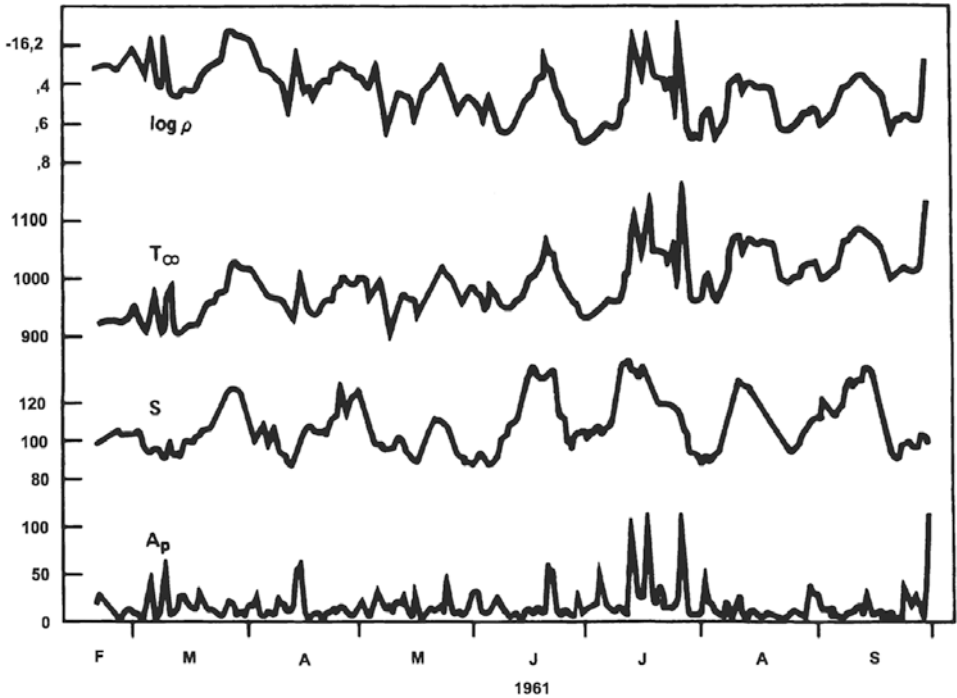


Figure 2.11. A comparison between thermospheric mass density ρ , exospheric temperature T_∞ , the solar 10.7 cm radio flux index S ($F_{10.7}$), and the A_p index as a function of time for 1961. (From Giraud and Petit, 1978.)

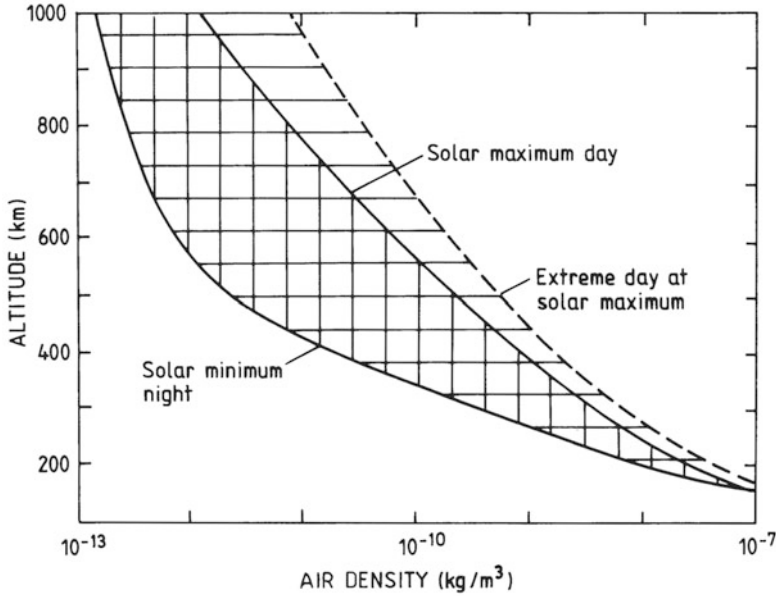


Figure 2.12. Illustration showing the extreme variability in the neutral density of the thermosphere under solar minimum and solar maximum conditions.

Satellites at these altitudes will experience great differences in the friction force due to atmospheric drag in response to these density variations, and during severe disturbances the satellite trajectories can be altered significantly. It is therefore of great importance to know the behavior of the upper atmosphere when planning space missions, because an unexpected atmospheric disturbance can reduce the lifetime of a satellite by several months, if not destroy the mission completely.

We also notice from [Figure 2.11](#) that the geomagnetic activity due to enhanced ionospheric currents can give rise to abrupt changes in exospheric temperature as well as density; again, this is one of the main reasons for the interest in geomagnetic disturbances as it has practical importance for satellite trajectories. These disturbances are also the most difficult to predict because geomagnetic disturbances occur in a very erratic manner especially at high latitudes.

Let us therefore consider the effect of variations in atmospheric density on a satellite orbit. For a sphere with mass m moving with velocity v with respect to atmospheric gas, there will be a drag force F_D acting on the sphere due to collisions with atmospheric particles, which can be expressed in the following way:

$$F_D = \frac{1}{2} \rho v^2 C_D$$

where ρ is atmospheric gas density, and C_D is what is called the ballistic coefficient. It is proportional to the cross-section of the sphere, and depends on surface conditions of the sphere's material.

For a satellite moving in a circular orbit with radius r around the Earth the total energy is:

$$E = \frac{1}{2}mv^2 - \frac{GM_em}{r}$$

where G is the constant of gravity, and M_e the mass of the Earth.

If the atmospheric drag is small, the circular orbit will be maintained and then for circular orbits:

$$\frac{v^2}{r} = \frac{GM_e}{r^2} \quad (2.1)$$

The total energy of the satellite moving in a circular orbit in a central force field therefore is given by:

$$E = -\frac{GM_em}{2r} \quad (2.2)$$

The rate of change of energy for the satellite due to atmospheric drag can be expressed as:

$$\frac{dE}{dt} = -F_D v = -\frac{1}{2}\rho v^3 C_D \quad (2.3)$$

By deriving dE/dt from (2.2) and equating it to (2.3) we have:

$$\frac{dE}{dt} = \frac{GM_em}{2r^2} \frac{dr}{dt} = -\frac{1}{2}\rho v^3 C_D$$

and when applying (2.1) the rate of change of the radius of the orbit is

$$\frac{dr}{dt} = -\frac{\rho v C_D \cdot r}{m} \quad (2.4)$$

By observing the rate of change of the orbit's radius one could now derive the atmospheric density or, vice versa, when the atmospheric density is known the expected rate of change of the orbital radius could be obtained. Since variations in r from orbit to orbit are very small, it is not so practical to use (2.4) to study the effects on satellite orbits from atmospheric drag. It turns out that the orbital period ($T = 2\pi r/v$) is a better parameter for this.

According to Kepler's third law we have:

$$T^2 = \frac{4\pi^2 r^3}{GM_e}$$

By taking the time derivative

$$2T \frac{dT}{dt} = \frac{12\pi^2 r^2}{GM_e} \frac{dr}{dt} = \frac{12\pi^2 r}{v^2} \frac{dr}{dt}$$

and solving for dT/dt

$$\frac{dT}{dt} = \frac{6\pi^2 r}{Tv^2} \frac{dr}{dt}$$

we find by inserting (2.4) and solving for $dT/dt \equiv \dot{T}$:

$$\dot{T} \equiv \frac{dT}{dt} = -\frac{3\pi C_D r}{m} \rho$$

The period therefore decreases faster as the density increases. This can appear as an acceleration of the satellite, but since the energy is constant, the gain in kinetic energy must be lost by a reduction in potential energy due to the reduction in orbital radius by increasing neutral density.

Measuring the amount of change of the rotation period of the satellite is much easier than measuring the rate of change of the radius, and it can actually be used to derive the atmospheric density at the satellite altitude.

In [Figure 2.13](#) the variation in the rotation periods of the satellites Explorer IV and Vanguard I is compared for a few months in 1958–1959. A close correlation in the variations is shown indicating that the effect is not local but global. Furthermore, it is demonstrated in the lower panel of [Figure 2.13](#) that these variations in the case of Sputnik III are correlated with variations in the solar sunspot number. These observations are interpreted as due to variations in atmospheric density above altitudes of 300 km due to expansion and contraction caused by variations in solar heat input.

[Figure 2.14](#) illustrates the rate of changes in seconds per day of the orbital period as a function of solar heat input for satellites at different altitudes. The 10.7 cm radio emission flux ($F_{10.7}$) is used as a parameter for solar heat input. At lower altitudes the rate of change becomes more severe for higher solar fluxes.

2.4 THE ATMOSPHERE AS AN IDEAL GAS

Consider the forces on a small mass element dm of air ([Figure 2.15](#)) at a height z above the ground. Let the mass element take the form of a small cylinder with horizontal cross-section A and height dz . This air mass will be acted upon by gravity, and this force can be expressed as

$$df = -nmgA dz$$

where g is the acceleration of gravity, and n is the number density of the molecules with mass m . In static equilibrium the gravity force must be balanced by the net pressure force in the following way:

$$[p - (p + dp)]A - nmgA dz = 0$$

where p is the pressure, which gives:

$$\frac{dp}{dz} = -nmg = -\rho g \quad (2.5)$$

Here $\rho = nm$ is the mass density. Equation (2.5) is called the barometric law. Assuming that the atmosphere is an ideal gas which is a very good assumption at

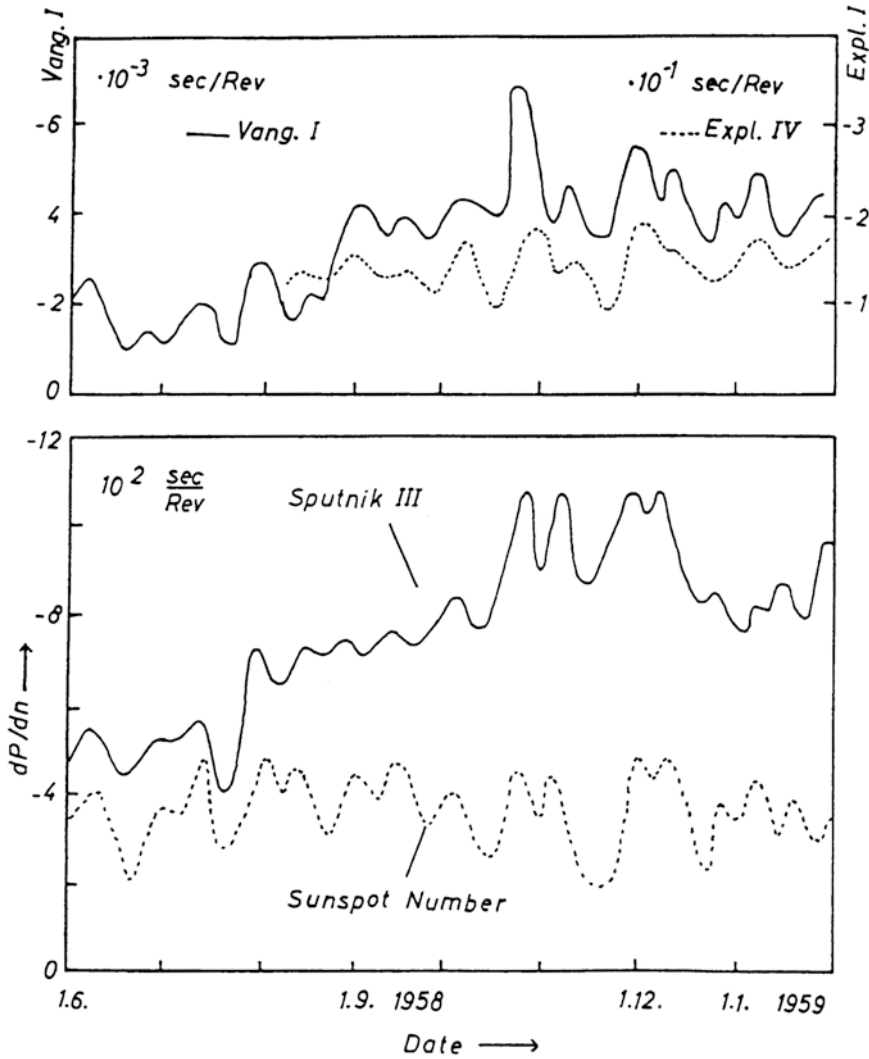


Figure 2.13. (Upper panel) The rate of change in orbital period per period for Explorer IV and Vanguard I satellites between June 1958 and February 1959. (Lower panel) A correlation between the variations in orbital periods for Sputnik III and sunspot numbers for the same period as above. (From Paetzold and Zschörner, 1960.)

least for the lower parts of the atmosphere, then we can apply the ideal gas law $p = nkT$ and derive from (2.5)

$$\frac{1}{p} \frac{dp}{dz} = -\frac{nmg}{nkT} = -\frac{mg}{kT} = -\frac{1}{H} \quad (2.6)$$

The parameter $H = kT/mg$ is called the scale height.

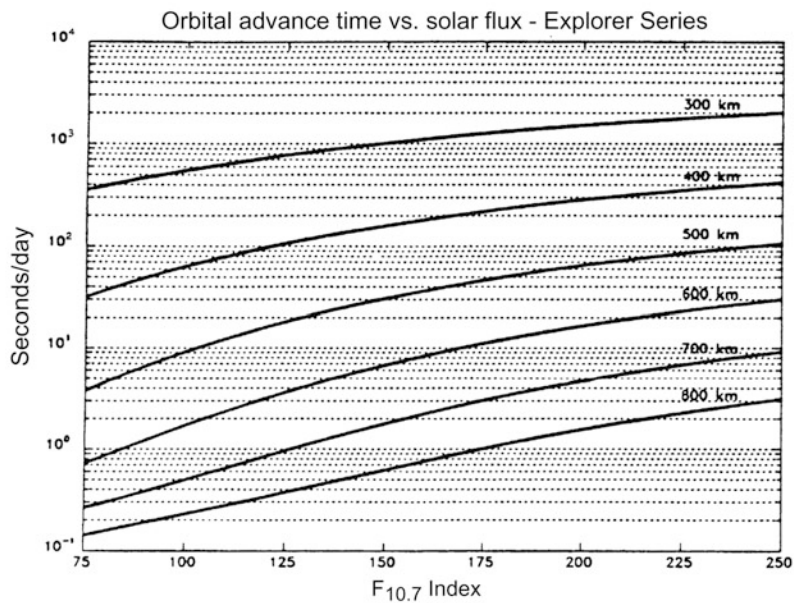


Figure 2.14. The rate of change in orbital period per day as a function of solar flux at 10.7 cm radio emission ($F_{10.7}$) for satellites at different heights between 300 and 800 km. (From Walterscheid, 1989.)

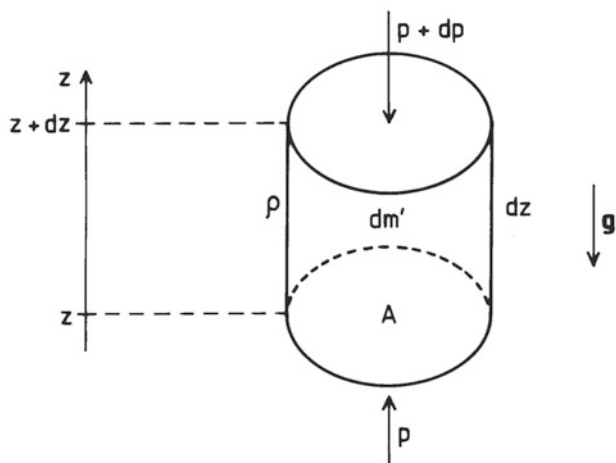


Figure 2.15. A volume element of air used to illustrate the balance between pressure and gravity forces.

We recall from kinetic gas theory that according to the equipartition principle each degree of freedom gives rise to a kinetic energy equal to $\frac{1}{2}kT$. We then notice that if all this kinetic energy in the vertical direction is converted to potential energy, the molecule must be lifted a height h given by:

$$\left. \begin{aligned} mgh &= \frac{1}{2}mv_z^2 = \frac{1}{2}kT \\ h &= \frac{1}{2} \frac{kT}{mg} = \frac{1}{2}H \end{aligned} \right\} \quad (2.7)$$

where v_z is the vertical velocity. This height then corresponds to half the scale height. Whether a particle will reach this height or not depends on its velocity and rate of collision. All in all, in thermal equilibrium there will always be a balance between the kinetic and potential energies of the particles so that the velocity distribution is kept constant at all heights. Only density will decrease in an isothermal atmosphere as will be shown below.

The pressure at any height can now be found by integrating (2.6):

$$\ln p = -\frac{z}{H} + \text{const.}$$

If $p = p_0$ at a reference height z_0 , we have:

$$p = p_0 \exp\left(-\frac{z - z_0}{H}\right) \quad (2.8)$$

For a constant temperature and a constant molecular mass the scale height is constant as long as the acceleration of gravity is constant. Close to Earth, where $T = 288$ K, $M' = 28.8$ is the mean molecular mass number, and $m = M' \cdot m_0$ is the mean mass of the molecules, where $m_0 = 1$ a.m.u. $= 1.660 \times 10^{-27}$ kg, $H = 8.47$ km. Since the temperature between the ground and 100 km altitude vary quite markedly, the scale height will vary between 5.0 and 8.3 km (see [Figure 2.1](#)) in this region. Above 100 km, however, the temperature increases drastically, and the molecules dissociate so that the molecular mass decreases. The scale height increases and the pressure therefore does not decrease as rapidly above 100 km as below. At 300 km, for example, at a temperature of 980 K and with molecular mass number of 16 we find $H \approx 50$ km.

Since $p = nkT$, we find an expression for the mass density by:

$$\rho = n \cdot m = \frac{m}{kT} \cdot p \quad (2.9)$$

We see that for a constant temperature and mean mass of the molecules, the mass density will decrease exponentially at the same rate as the pressure.

Let us consider for a while the number density when the atmosphere is isothermal. From the ideal gas law and the expression of the pressure (2.8) we have

$$p = nkT = p_0 \exp\left[-\frac{z - z_0}{H}\right] = n_0 k T_0 \exp\left[-\frac{z - z_0}{H}\right] \quad (2.10)$$

where n_0 and T_0 are the number density and temperature at the reference height

z_0 , respectively. Since the atmosphere is assumed isothermal, we see that

$$n = n_0 \exp\left[-\frac{z - z_0}{H}\right] \quad (2.11)$$

When the reference height is set at the ground level $z_0 = 0$, the total sum of all particles from the ground to infinity above a unit area on Earth is given by:

$$\mathcal{N} = \int_0^\infty n \, dz = n_0 \int_0^\infty \exp\left(-\frac{z}{H}\right) dz = n_0 H \quad (2.12)$$

We therefore see that the scale height is equivalent to the height the atmosphere would have if the atmosphere encircling the Earth had a constant density by height. It would then reach only 8.4 km above our heads, and outside there would be a vacuum. This is the reason people in the old days believed that the atmosphere was 8–10 km thick. They knew that the air pressure balanced a water column of about 10 m, and by knowing the ratio between the density of water (10^3 kg/m^3) and the density of air at ground level (1.2 kg/m^3), the height of the atmospheric “lid” would be

$$h_a = \frac{10^3 \text{ kg/m}^3}{1.2 \text{ kg/m}^3} \cdot 10 \text{ m} = 8.3 \text{ km}$$

Realizing that the atmosphere was not finite really opened up the universe to human beings.

For an isothermal atmosphere with constant molecular mass the mass density is given by:

$$\rho = \rho_0 \exp(-z/H) \quad (2.13)$$

2.5 THE EXOSPHERE

The ordinary gas law can only be applied to atmospheric gas as long as the molecules make enough collisions to establish statistical equilibrium with their surroundings. Let us assume that a molecule traveling vertically at the most probable velocity (see Exercise 2) $v_{mp} = \sqrt{2kT/m}$ without experiencing any collisions, then we have according to (2.7):

$$mgh_e = \frac{1}{2}mv_{mp}^2 = kT$$

and the molecule will reach a height h_e given by:

$$h_e = \frac{kT}{mg} = H$$

where H is the scale height. If this distance h_e was less than the mean free path, l , which is the distance between two collisions, the molecule could on average be considered to move freely. The part of the atmosphere where the scale height is of the same order as, or less than, the mean free path is called the exosphere.

The mean free path is given approximately as

$$l = \frac{1}{\sigma \cdot n}$$

where σ is the cross-section for collisions, and n is the number density of the atmosphere. We then notice at the exobase, which is the bottom of the exosphere and where $H = l$, that:

$$H \cdot n = \frac{1}{\sigma}$$

From (2.12) we find that:

$$H \cdot n = \mathcal{N}$$

where \mathcal{N} is the total number of particles per unit area above the height where the number density is n . We therefore have at the exobase that:

$$\mathcal{N} \cdot \sigma = 1$$

One such particle will therefore experience exactly one collision on its way up to the exobase. If $H < l$, the particle will not on average experience such a collision at all.

Most particles entering the exosphere from below travel in gravity-controlled orbits (ballistic motion) without making collisions until they either escape or return back to the atmosphere below. If a particle escapes from the Earth's gravitational field, its kinetic energy must be larger than its potential energy at the height of escape. Therefore

$$\frac{1}{2}mv^2 > mg_r r$$

where g_r is the acceleration of gravity at the distance of escape r , measured from the center of the Earth.

$$v > \sqrt{2g_r \cdot r} = \sqrt{2g_0 R_e^2 \frac{1}{r}} = v_{\text{esc}}$$

where g_0 is the acceleration of gravity at the Earth surface ($= 9.80 \text{ m/s}^2$). At the Earth's surface $v_{\text{esc}} = 11.2 \text{ km/s}$, while for larger distances v_{esc} becomes smaller. At about 2,000 km $v_{\text{esc}} \approx 9.7 \text{ km/s}$.

2.6 HEIGHT-DEPENDENT TEMPERATURE

We have shown in [Figures 2.1](#) and [2.3](#) that the temperature in the lower atmosphere (below, say, 100 km) varies by height, and therefore it is strictly not legitimate to assume that T is constant. Let us therefore express T as a linearly varying function with height

$$T = T_0 + \alpha \cdot z$$

α is often called the linear “lapse rate”. α can be positive as in the stratosphere and thermosphere and negative as in the troposphere and the mesosphere.

Introducing T in (2.6), but still assuming an ideal gas, we find:

$$\frac{dp}{p} = -\frac{mg}{kT} dz = -\frac{T_0}{H_0} \frac{dz}{T_0 + \alpha z}$$

where $H_0 = kT_0/mg$ is the scale height referring to $z = 0$. Solving this equation for p we find

$$\ln \frac{p}{p_0} = -\frac{T_0}{H_0} \int_0^z \frac{dz}{T_0 + \alpha z} = -\frac{T_0}{H_0 \alpha} \ln \left(\frac{T}{T_0} \right) = -\frac{mg}{k\alpha} \ln \frac{T}{T_0}$$

Therefore

$$\frac{p}{p_0} = \left(\frac{T}{T_0} \right)^{-mg/k\alpha} \quad (2.14)$$

By inserting (2.14) into (2.9) we get:

$$\rho = \frac{m}{kT} \cdot p_0 \left(\frac{T}{T_0} \right)^{-mg/k\alpha} = \rho_0 \left(\frac{T}{T_0} \right)^{-1-(mg/k\alpha)}$$

Therefore

$$\frac{\rho}{\rho_0} \neq \frac{p}{p_0}$$

Pressure and density for a non-isothermal atmosphere will not have the same variation profile by altitude.

Another complication to be mentioned here is variation in the acceleration of gravity

$$g(z) = g_0 \left(\frac{R_e}{R_e + z} \right)^2$$

where R_e is the Earth radius and g_0 is the acceleration of gravity at the Earth's surface. For $z < 100$ km this variation will contribute to a variation in H by only 3%. For $z = 1,000$ km, however, the error will be significant when neglecting the variation in g ($\approx 25\%$).

2.7 THE ADIABATIC LAPSE RATE

Assume that when a volume element in the atmosphere moves in altitude, the motion will occur without any exchange of heat with the surrounding atmosphere. This can happen if the motion is rapid enough. We then have the following adiabatic relationship for p and T :

$$Tp^{(1-\gamma)/\gamma} = \text{const.} \quad (2.15)$$

where $\gamma (= c_p/c_v)$ is the adiabatic constant, and $c_v = 712$ J/kg K and $c_p = 996$ J/kg K are the specific heat for air at constant volume and constant pressure, respectively. By differentiating (2.15) with respect to z we find

$$\frac{\partial T}{\partial z} = + \frac{\gamma - 1}{\gamma} \frac{T}{p} \frac{\partial p}{\partial z}$$

By introducing (2.6)

$$\frac{\partial T}{\partial z} = - \frac{\gamma - 1}{\gamma} \frac{mg}{k} = \alpha^* \quad (2.16)$$

where α^* is called the adiabatic “lapse rate”.

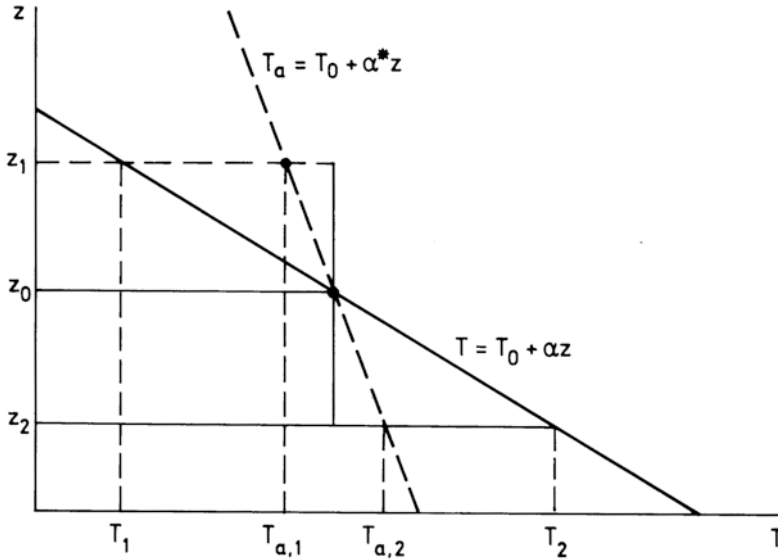


Figure 2.16. Atmospheric temperature T as a function of height with a lapse rate α as compared with temperature representing the adiabatic lapse rate α^* for an unstable atmosphere.

At the Earth's surface $\gamma = 1.4$ and therefore

$$\alpha^* = -9.8 \text{ K/km}$$

Temperature decreases by almost 1 K per 100 m elevation at ground level.

Let us now assume that we have an atmosphere where the temperature within a certain height region decreases more rapidly than the adiabatic lapse rate (Figure 2.16).

If we now imagine a small bubble of air ascending from height z_0 to height z_1 without heat exchange with the environment, then the temperature of the bubble will follow the adiabatic temperature illustrated by T_a to the temperature $T_{a,1}$ which is above the temperature T_1 in the atmosphere itself at height z_1 . Therefore, the air bubble will be lighter than the surrounding air and the bubble will continue to ascend.

If, on the other hand, the bubble at z_0 starts to descend to z_2 without heat exchange with the surroundings, the temperature in the bubble will be $T_{a,2}$ according to the adiabatic temperature. The temperature in the bubble will therefore be less than in the surrounding air, and the bubble becomes heavier and continues to sink. In a situation where the temperature of the air decreases more rapidly than the adiabatic lapse rate, the air is unstable.

For the opposite sense, when the temperature in the atmosphere decreases more slowly than the adiabatic lapse rate as illustrated in Figure 2.17, the atmosphere becomes stable.

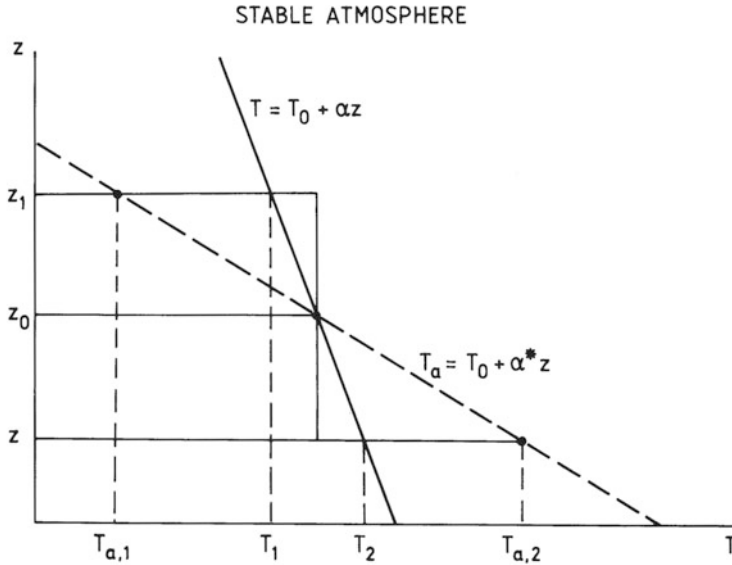


Figure 2.17. The same as in Figure 2.16 except the atmosphere is stable.

Small disturbances in the atmosphere are usually adiabatic. The most likely areas for an unstable atmosphere, however, are the regions of the atmosphere where the temperature decreases (i.e., in the troposphere and the mesosphere which are also the regions where turbulence is most prominent). In the stratosphere, where the temperature increases, the atmosphere is stable.

2.8 DIFFUSION

We have seen from Figure 2.2 that above 100 km the densities of different species decay according to individual scale heights. This comes about because above the mesopause the temperature increases and the atmosphere is stabilized; turbulence does not take place, and the different species are no longer homogeneously mixed. They will therefore distribute themselves according to the barometric law (2.5) with individual scale heights as if they were the only gas.

Sometimes, however, it is of interest to study the situation where the main gas, the major constituent, is distributed according to its specific scale height while another gas, a minor constituent, represented by a smaller density is moving through the majority one at a velocity that is determined by diffusion.

Assume first that there is no gravitational field and the majority gas is at rest and uniformly distributed. Let the minority gas with mean mass per molecule m be distributed by its density n , where there is a gradient dn/dx along the x -axis. Because of this gradient in the gas density the molecules will move down the

gradient at a speed v , and the particle flux $\phi = nv$ will be proportional to this gradient (Fick's law):

$$\phi = nv = -D \cdot \frac{\partial n}{\partial x} \quad (2.17)$$

where D is what we will call the diffusion coefficient with dimension m^2/s .

From the equation of continuity for a gas we have:

$$\frac{\partial n}{\partial t} + \frac{\partial}{\partial x}(nv) = 0$$

or when inserting (2.17)

$$\frac{\partial n}{\partial t} = -\frac{\partial}{\partial x}(nv) = \frac{\partial}{\partial x} \left(D \frac{\partial n}{\partial x} \right) \quad (2.18)$$

For a constant diffusion coefficient with respect to x we get:

$$\frac{\partial n}{\partial t} = D \frac{\partial^2 n}{\partial x^2}$$

which is the rate of change of the gas density at a given point in space. This is the diffusion equation for the gas density n .

Because of the gradient in the minority gas density, there will be a pressure force acting on the gas although the temperature is constant, and this is given by:

$$F_p = -\frac{\partial p}{\partial x} = -kT \frac{\partial n}{\partial x} \quad (2.19)$$

where it is assumed an ideal gas. If now each of the minority particles experiences ν collisions per unit time with the majority gas which is at rest, there will be a restoring force:

$$F_\nu = -nm\nu v$$

which, when no other force is acting, must balance the pressure force (2.19). Thus

$$-kT \frac{\partial n}{\partial x} - nm\nu v = 0$$

and

$$nv = -\frac{kT}{m\nu} \frac{\partial n}{\partial x} = -D \frac{\partial n}{\partial x}$$

A simple expression for the diffusion coefficient now emerges:

$$D = \frac{kT}{m\nu} \quad (2.20)$$

Since the collision frequency between the minority and the majority gas is proportional to the density of the majority gas, n_M , and the square root of the temperature which is the same for the two gases:

$$\nu \propto n_M T^{1/2}$$

the diffusion coefficient obeys the following proportionality

$$D \propto T^{1/2} n_M^{-1}$$

Diffusion therefore increases with temperature and decreases with density n_M .

Let now the space coordinate be vertical and assume that the gravity force mg is acting downward on each volume of the minority constituent, then the collisions must balance the sum of the pressure and gravity forces as follows:

$$-\frac{\partial p}{\partial z} - nmg = nm\nu w$$

where w is the vertical velocity. Then again for an ideal gas:

$$-kT \frac{\partial n}{\partial z} - nmg = nm\nu w$$

and solving for the vertical flux we get

$$nw = -\frac{kT}{m\nu} \left(\frac{\partial n}{\partial z} + \frac{gm}{kT} n \right) = -D \left(\frac{\partial n}{\partial z} + \frac{n}{H_m} \right) \quad (2.21)$$

D is given by (2.20), and $H_m = kT/mg$ is the scale height of the minority constituent. We notice that H_m enters the equation as a constant and does not need to be equal to the distribution height $[-(1/n)(\partial n/\partial z)]^{-1}$ of the minority gas.

Now, when applying (2.18) for vertical motion and inserting (2.21) for nw :

$$\frac{\partial n}{\partial t} = -\frac{\partial}{\partial z}(nw) = \frac{\partial}{\partial z} \left\{ D \left(\frac{\partial n}{\partial z} + \frac{n}{H_m} \right) \right\} \quad (2.22)$$

From (2.20) we have that $D = kT/m\nu$, and since ν must be proportional to the density n_M of the majority constituent which is distributed according to the scale height H_M , we get:

$$\nu \propto n_M = n_{M_0} \exp(-z/H_M)$$

The diffusion coefficient can then be expressed as:

$$D = D_0 \exp(z/H_M) \quad (2.23)$$

It increases exponentially with height in an isothermal atmosphere. By inserting this expression for D into (2.22) we get:

$$\begin{aligned} \frac{\partial n}{\partial t} &= \left(\frac{\partial n}{\partial z} + \frac{n}{H_m} \right) \frac{\partial D}{\partial z} + D \left(\frac{\partial^2 n}{\partial z^2} + \frac{1}{H_m} \frac{\partial n}{\partial z} \right) \\ &= D \left\{ \frac{\partial^2 n}{\partial z^2} + \left(\frac{1}{H_M} + \frac{1}{H_m} \right) \frac{\partial n}{\partial z} + \frac{n}{H_M H_m} \right\} \end{aligned}$$

If it is assumed that at a particular height z the density of the minority constituent is distributed according to the exponential function

$$n = n_0 \exp(-z/\delta) \quad (2.24)$$

where δ is the local scale height; then at this height z the density will change by time at a rate:

$$\begin{aligned}\frac{\partial n}{\partial t} &= D \left\{ +\frac{1}{\delta^2} - \left(\frac{1}{H_m} + \frac{1}{H_M} \right) \frac{1}{\delta} + \frac{1}{H_M H_m} \right\} n \\ &= D \left\{ \left(\frac{1}{\delta} - \frac{1}{H_m} \right) \left(\frac{1}{\delta} - \frac{1}{H_M} \right) \right\} n \\ &= \Gamma \cdot n\end{aligned}$$

As long as the density of the minority constituent remains approximately exponentially distributed by distribution height δ , its concentration will vary in time at altitude z by the rate $\Gamma \cdot n$ where Γ is given by:

$$\Gamma = D \left\{ \left(\frac{1}{\delta} - \frac{1}{H_m} \right) \left(\frac{1}{\delta} - \frac{1}{H_M} \right) \right\}$$

This result, however, deserves some comments. In [Table 2.1](#) we show the different values that δ can take in relation to H_M and H_m and the following values of Γ/D .

In most cases of δ , H_m and H_M are roughly of the same order of magnitude (Ratcliffe, 1972). There are two situations, however, where $\partial n/\partial t = 0$ or $\Gamma = 0$ (i.e., steady state). First, when $\delta = H_m$ or the minority constituent is distributed according to its natural scale height in (2.24). There will then according to (2.21) be no vertical motion because

$$w = -D \left(-\frac{1}{H_m} + \frac{1}{H_m} \right) = 0$$

Table 2.1. Time constants for loss by diffusion. (From Ratcliffe, 1972.)

<i>Value of δ</i>	<i>Approximate value of Γ/D</i>
$\delta > H_m$ and $\delta > H_M$	$1/H_M \cdot H_m$
$\delta = H_m$	0
$\delta > H_M$ and $\delta < H_m$	$-1/\delta \cdot H_M$
$\delta < H_M$ and $\delta > H_m$	$-1/\delta \cdot H_m$
$\delta = H_M$	0
$H_m > \delta$ and $H_M > \delta$	$1/\delta^2$
$\delta < 0$	$> 1/H_M \cdot H_m$

everywhere. The second case appears when $\delta = H_M$ in (2.24); the minority gas is distributed according to the scale height of the majority gas. Then, according to (2.21)

$$w = +D \left(+\frac{1}{H_M} - \frac{1}{H_m} \right) \neq 0$$

and w is positive if $H_m > H_M$, otherwise it is negative. The number of particles crossing a unit area per unit time will be according to (2.21):

$$nw = +nD \left(+\frac{1}{H_M} - \frac{1}{H_m} \right) = n_0 D_0 \left(\frac{1}{H_M} - \frac{1}{H_m} \right)$$

where we have inferred D from (2.23) and n from (2.24) when $\delta = H_M$. The upward decrease in n ($\approx \exp(-z/H_M)$) is just equal to the upward increase in D ($\approx \exp(z/H_M)$) so that there is a steady flow of gas upwards or downwards depending on whether H_m is greater or smaller than H_M . In spite of the fact that $\partial n / \partial t = 0$ the situation is therefore not one of dynamic equilibrium.

2.9 THE EQUATION OF MOTION OF THE NEUTRAL GAS

Since we are going to discuss the motion of the atmosphere of a rotating planet, it is convenient to express the kinetic equations in a reference frame rotating with the planet at an angular velocity $\mathbf{\Omega}$. We start out with the general equation of motion for a neutral gas

$$\frac{d\mathbf{u}}{dt} = -\frac{1}{\rho} \nabla p + \mathbf{g} + \mathbf{f} \quad (2.25)$$

Here we have split up the external force into the pressure force, the force of gravity, \mathbf{g} , and any other accelerating force, \mathbf{f} , per unit mass.

We now denote by \mathbf{u}_f the velocity observed in an inertial frame of reference (e.g., one fixed to the center of the Earth). The velocity \mathbf{u}_r , observed in a reference frame rotating with an angular velocity $\mathbf{\Omega}$ around an axis through the center of the Earth and at a distance \mathbf{r} from this center, is according to the laws of mechanics related to \mathbf{u}_f by (Figure 2.18):

$$\left(\frac{d\mathbf{r}}{dt} \right)_f = \left(\frac{d\mathbf{r}}{dt} \right)_r + \mathbf{\Omega} \times \mathbf{r}$$

and

$$\mathbf{u}_f = \mathbf{u}_r + \mathbf{\Omega} \times \mathbf{r}$$

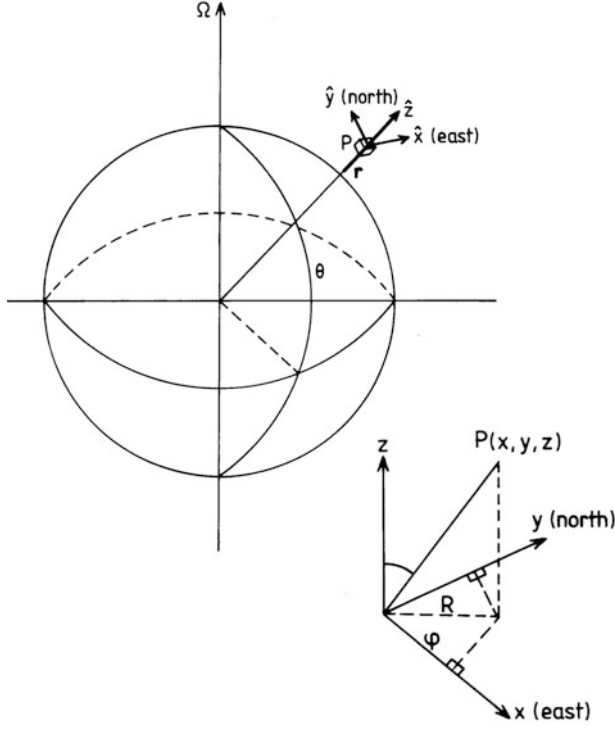


Figure 2.18. The coordinate system used to describe the motion of an air parcel at a distance r from the Earth's center and rotating with the Earth at an angular velocity Ω .

The acceleration of this air parcel in the fixed frame of reference is now, since Ω is constant, given by:

$$\begin{aligned}
 \mathbf{a}_f &= \left(\frac{d\mathbf{u}_f}{dt} \right)_f = \left(\frac{d}{dt} (\mathbf{u}_r + \Omega \times \mathbf{r}) \right)_f \\
 &= \left(\frac{d}{dt} \mathbf{u}_r \right)_f + \left(\frac{d}{dt} (\Omega \times \mathbf{r}) \right)_f \\
 &= \left(\frac{d\mathbf{u}_r}{dt} \right)_r + \Omega \times \mathbf{u}_r + \Omega \times \left(\frac{d\mathbf{r}}{dt} \right)_f \\
 &= \mathbf{a}_r + \Omega \times \mathbf{u}_r + \Omega \times \mathbf{u}_r + \Omega \times (\Omega \times \mathbf{r}) \\
 &= \mathbf{a}_r + 2\Omega \times \mathbf{u}_r + \Omega \times (\Omega \times \mathbf{r})
 \end{aligned}$$

where \mathbf{a}_r is acceleration in the rotating reference frame. This acceleration can be expressed as

$$\mathbf{a}_r = \mathbf{a}_f - 2\Omega \times \mathbf{u}_r - \Omega \times (\Omega \times \mathbf{r})$$

Since the equation of motion in the fixed frame of reference is given by

$$\mathbf{a}_f = \left(\frac{d\mathbf{u}}{dt} \right)_f = -\frac{1}{\rho} \nabla p + \mathbf{g} + \mathbf{f}$$

the equation of motion in a reference system following the Earth's rotation becomes

$$\mathbf{a} = \frac{d\mathbf{u}}{dt} = -\frac{1}{\rho} \nabla p + \mathbf{g} + \mathbf{f} - 2\boldsymbol{\Omega} \times \mathbf{u} - \boldsymbol{\Omega} \times (\boldsymbol{\Omega} \times \mathbf{r})$$

when deleting the index r . Expanding the final vector product we have

$$\frac{d\mathbf{u}}{dt} = -\frac{1}{\rho} \nabla p + \mathbf{g} + \mathbf{f} - 2\boldsymbol{\Omega} \times \mathbf{u} - (\boldsymbol{\Omega} \cdot \mathbf{r})\boldsymbol{\Omega} + \Omega^2 \mathbf{r}$$

It is then customary to introduce the potential function

$$\chi = -\mathbf{g} \cdot \mathbf{r} - \frac{1}{2} \Omega^2 r^2 \cos^2 \theta$$

where θ is the latitude angle and r the radial distance to the point P as seen from the Earth's center (Figure 2.18).

Finally, the equation of motion takes the form:

$$\frac{d\mathbf{u}}{dt} + 2\boldsymbol{\Omega} \times \mathbf{u} + \frac{1}{\rho} \nabla p + \nabla \chi = \mathbf{f} \quad (2.26)$$

where $2(\boldsymbol{\Omega} \times \mathbf{u})$ is called the Coriolis acceleration, while $\boldsymbol{\Omega} \times (\boldsymbol{\Omega} \times \mathbf{r})$ is the centrifugal acceleration.

For an observer fixed on the Earth we have the rotation frequency $\Omega = 7.27 \times 10^{-5} \text{ s}^{-1}$ and, since the Earth radius is $R_e = 6.37 \times 10^6 \text{ m}$, we find $\Omega^2 R_e = 3.37 \times 10^{-2} \text{ m/s}^2$ which represents the maximum centrifugal acceleration (at the equator). This can be neglected as it is much smaller than $g = 9.81 \text{ m/s}^2$.

We note that in the northern hemisphere the Coriolis force will tend to deflect motion to the right of the direction of the velocity vector. The Coriolis force is quite weak since for a velocity of 1,000 m/s, which is very high for neutral air velocity, the maximum acceleration corresponds to $1.49 \times 10^{-2} g$. For motions persisting over long periods, however, the deflection of velocity is quite important and creates, in meteorological terms, cyclones in the northern hemisphere. These are important elements in the weather system. For practical reasons we will now choose a Cartesian coordinate system (x, y, z) fixed on the Earth's surface as indicated in Figure 2.18 and denote the velocity components (u, v, w) along the different axes. u , v , and w are counted positive eastward, northward, and upward, respectively. Since we have neglected centrifugal force, the acceleration of gravity is given by

$$\mathbf{g} = -g\hat{\mathbf{z}}$$

The angular velocity vector is given by:

$$\boldsymbol{\Omega} = \Omega \sin \theta \hat{\mathbf{z}} + \Omega \cos \theta \hat{\mathbf{y}}$$

From (2.26) we find for each component of the acceleration:

$$\frac{du}{dt} - 2\Omega v \sin \theta + 2\Omega w \cos \theta + \frac{1}{\rho} \frac{\partial p}{\partial x} = f_x \quad (2.27a)$$

$$\frac{dv}{dt} + 2\Omega u \sin \theta + \frac{1}{\rho} \frac{\partial p}{\partial y} = f_y \quad (2.27b)$$

$$\frac{dw}{dt} - 2\Omega u \cos \theta + \frac{1}{\rho} \frac{\partial p}{\partial z} + g = f_z \quad (2.27c)$$

2.10 GEOSTROPHIC AND THERMAL WINDS

We will now study some of the steady-state solutions ($d/dt = 0$) by assuming first of all that there is no vertical motion ($w = 0$), then that all other external forces except gravity are negligible and finally that the barometric law (2.5) applies; that is:

$$\frac{\partial p}{\partial z} = -\rho g = -nmg$$

where $\rho = n \cdot m$. For horizontal motion we obtain from (2.27) the so-called geostrophic wind solution:

$$u = -\frac{1}{2\rho\Omega \sin \theta} \frac{\partial p}{\partial y} \quad (2.28a)$$

$$v = \frac{1}{2\rho\Omega \sin \theta} \frac{\partial p}{\partial x} \quad (2.28b)$$

We notice that, since $\sin \theta = 0$ at the equator, there can be no geostrophic wind there. u and v change sign, however, across the equator. The geostrophic equations describe the motion of an air parcel that is initially moving from a high- to a low-pressure area. This motion is slow enough for the Coriolis force to deflect the air motion so that it finally becomes parallel to the isobars. We notice this because

$$\mathbf{v} \cdot \nabla p = u \frac{\partial p}{\partial x} + v \frac{\partial p}{\partial y} = 0$$

and v is perpendicular to the pressure gradients which by definition are perpendicular to the isobars.

By introducing the ideal gas law ($p = nkT$) in the geostrophic wind equations (2.28) we find the so-called thermal wind equation:

$$\frac{u}{T} = -\frac{k}{2m\Omega \sin \theta} \frac{\partial}{\partial y} (\ln p)$$

$$\frac{v}{T} = +\frac{k}{2m\Omega \sin \theta} \frac{\partial}{\partial x} (\ln p)$$

By now differentiating with respect to height we obtain, when $p = p_0 \exp(-z/H)$ from (2.8) and $z_0 = 0$:

$$\frac{\partial}{\partial z} \left(\frac{u}{T} \right) = - \frac{g}{2\Omega T^2 \sin \theta} \frac{\partial T}{\partial y}$$

$$\frac{\partial}{\partial z} \left(\frac{v}{T} \right) = + \frac{g}{2\Omega T^2 \sin \theta} \frac{\partial T}{\partial x}$$

These equations relate vertical wind shears in the geostrophic wind to horizontal gradients in the temperature.

Consider the northern hemisphere close to ground where it is hot at the equator and cold at the poles. Then, $\partial T / \partial y$ will be less than zero there so that $(\partial / \partial z)(u/T)$ becomes larger than zero. Up toward the tropopause therefore the meridional wind will increase eastward. Even if the wind is westward at the ground, it may become eastward at some height in the troposphere. In the southern hemisphere, because both $\partial T / \partial y$ as well as $\sin \theta$ change sign there, the wind will also increase towards the east as one ascends in the troposphere.

In the stratosphere the situation can be different. The summer pole is continually heated at a higher temperature than at the equator which in turn is hotter than the totally unilluminated winter pole in the stratosphere. Thus, thermal winds in the stratosphere will have a seasonal dependence.

The wind pattern and temperature distribution up to the mesosphere is fairly well known and, except for the lowest 1,000 meters of the atmosphere, the zonal winds appear to be adequately described by the thermal wind equation (Murgatroyd, 1957). It is at about 65 km that the summer and winter temperatures are roughly equal. Above this height in the mesosphere the winter temperatures are higher.

There are also meridional prevailing winds leading to a net latitudinal flow of air which must be balanced by return flows at other heights. This will set up large meridional wind cells.

2.11 THE WIND SYSTEMS OF THE UPPER ATMOSPHERE

We will now discuss the wind system in the mesosphere and thermosphere. In [Figure 2.19](#) average zonal winds for January are shown below 130 km. We recognize the strong jet streams at the tropopause. Note that by meteorological usage E and W stands for easterly and westerly, which actually means winds coming from the east and west, respectively. This is the opposite sense to the convention in ionospheric physics where E and W means eastward- and westward-blowing winds, respectively.

In the mesosphere with its center around 60 km, however, there is a strong eastward-blowing wind in the winter hemisphere and a similar but weaker westward-blowing wind in the summer hemisphere. The maximum wind speed is observed close to 40° of latitude in both hemispheres. This wind pattern again

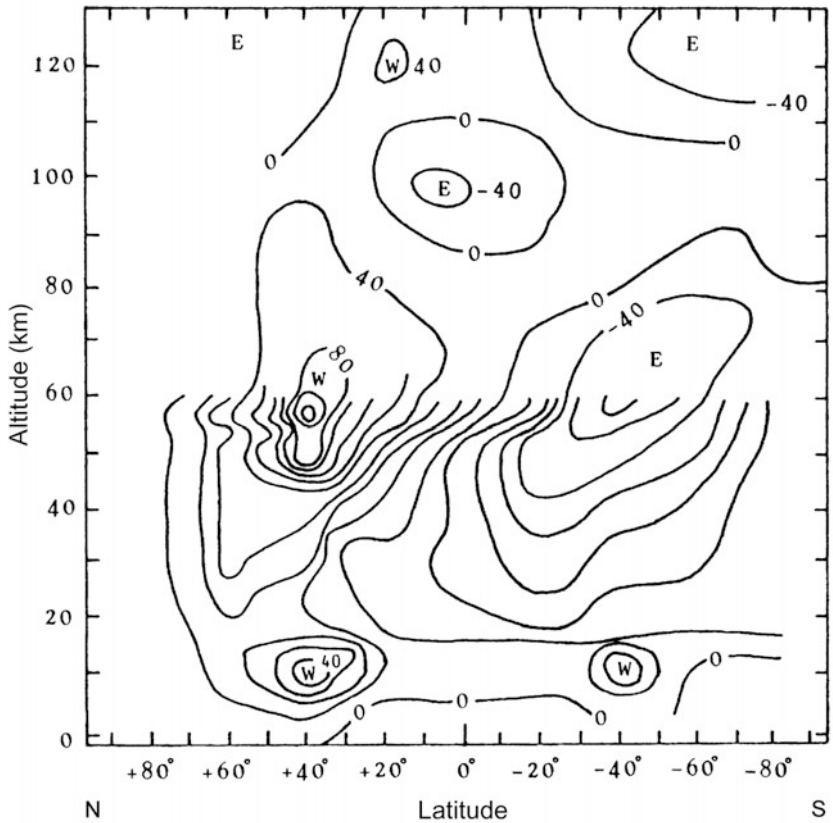


Figure 2.19. Zonal average east–west wind in January. Numerals on the contours are wind speed in units of m s^{-1} below 130 km altitude. Positive numbers represent eastward winds. Notice the meteorological convention of W representing westerly (i.e., winds coming from the west). (From Tohmatsu, 1990.)

appears to be well explained by the thermal wind equation. As can be seen from the temperature distribution presented in [Figure 2.20](#), the temperatures are high in the stratosphere in the summer hemisphere, while they are low in the winter hemisphere. The difference is about 50 K at about 40 km. In the mesosphere, however, the situation is the opposite where the temperature in the polar hemisphere at about 80 km is about 230 K, while it is less than 180 K in the summer hemisphere (as illustrated in [Figure 2.21](#) where the vertical temperature distribution as observed from Fort Churchill (59°N) in summer and winter are compared). In contrast to average zonal winds in the troposphere, which are eastward in both hemispheres, the average zonal winds in the mesosphere have opposite directions.

Meridional winds in the mesosphere appear to have an average net flow from the summer hemisphere to the winter hemisphere. Large variability in this height

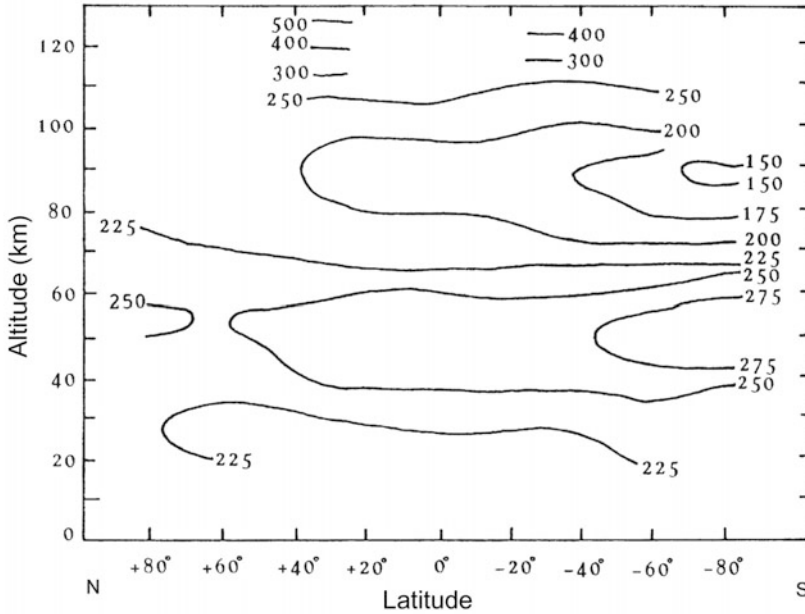


Figure 2.20. Meridional distribution of the mean atmospheric temperature in January. Numerals labeled on the contours are in kelvins. Notice that the mesosphere is warmer in wintertime than in summertime. (From Tohmatsu, 1990.)

region seems to be present as can be observed by comparing the schematic wind diagrams for 80 and 100 km, respectively, in [Figure 2.22](#).

2.12 OBSERVATIONS OF THE NEUTRAL WIND

While winds at the ground can be sensed by the human body and relatively easily measured, the wind at higher altitudes is a rather elusive parameter to observe. In the stratosphere and lower mesosphere our knowledge of the neutral wind has been derived from balloon and meteorological rocket measurements. One method quite often used has been observations of anomalous propagation of sound waves from small grenade detonations released by rockets. Higher up in the mesosphere and lower thermosphere meteor trail tracking by radars has produced considerable insight in the neutral wind system at these height regions. Observations of the motion of noctilucent clouds have also been used to deduce neutral winds in the mesopause region.

At higher altitudes in the lower thermosphere information about the neutral wind has, in addition to meteor trail observations, been derived from chemiluminescent cloud releases from rockets at twilight. Solar radiation that is resonance-scattered by alkali metal atoms can easily be observed from ground in

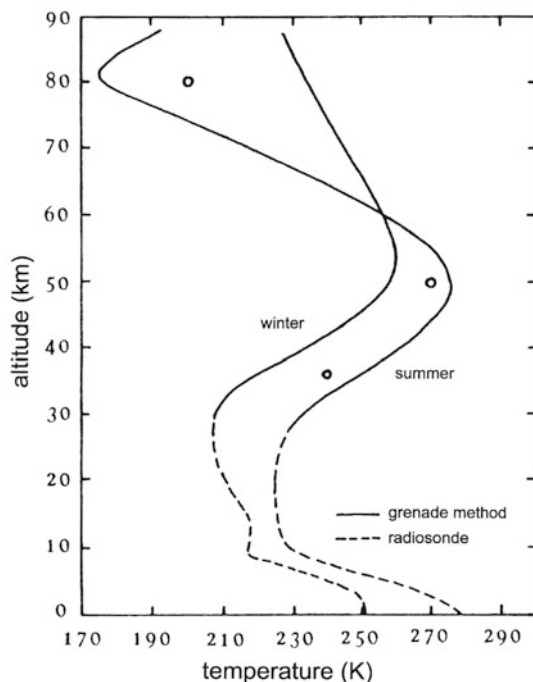


Figure 2.21. Vertical distributions of the mean atmospheric temperature in summer and winter measured at Fort Churchill (59° N). The solid and dashed curves are those measured by the grenade method and radiosondes, respectively. Open circles represent the average values at White Sands (23° N). (From Stroud *et al.*, 1959.)

clear weather. The extended height profiles of the neutral wind in the lower thermosphere can also be obtained by chemical trimethyl aluminum (TMA) releases from rockets. As these chemical releases have to be made at twilight, limited time coverage is available for these methods.

For F-region and partly also E-region neutral winds at high-latitude optical observations of the Doppler shift in auroral emission lines from oxygen can be used at high latitudes. But again the ability of the method to give extended time coverage of the winds is limited to the period of dark and clear polar sky. Optical Doppler measurements of airglow emissions have also been used to study F-region neutral winds at middle and lower latitudes.

The incoherent scatter method for deriving F-region and E-region neutral winds is a method that can give continuous coverage. This method, as we will see, is rather indirect and is still related to large uncertainties in the choice of model atmospheres especially at high latitudes.

In the upper thermosphere observations of atmospheric drag on satellites have been used to derive the temperature distribution in these higher regions, and from these again neutral wind patterns have been derived by applying these temperature

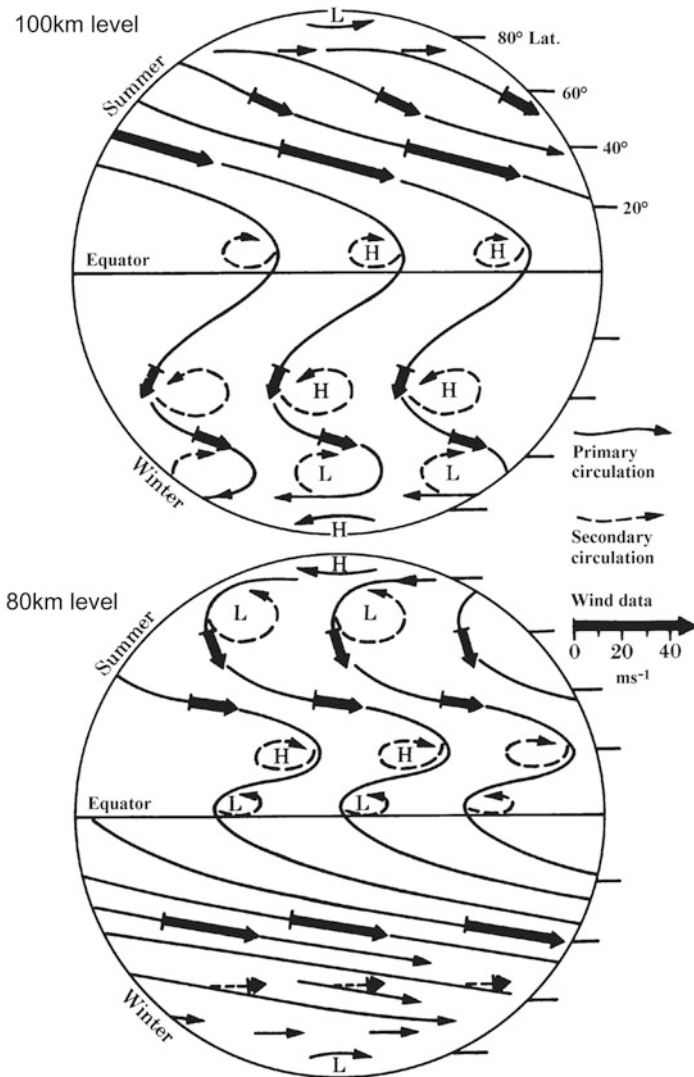


Figure 2.22. Schematic models of the planetary neutral air circulation at 80 and 100 km. (From Kochanski, 1963.)

observations as an input to the pressure term in the mobility equation of the neutral gas.

For E-region neutral winds, probably the most important basis for our understanding has been the analysis of geomagnetic variations on the ground. These have a very long history which has resulted in a larger amount of work attempting to resolve the different factors contributing to magnetic variations—one of the most important of these being the E-region neutral wind setup by tidal forces.

2.13 COLLISIONS BETWEEN PARTICLES

Let us assume a gas where we have two kinds of gas species, m and n , that are colliding with each other. Each collision must be related to a mutual force. Assume, for simplicity, that this force per unit mass acting on m -type particles due to the collision with n -type particles is proportional to the velocity difference $\mathbf{u}_m - \mathbf{u}_n$ between the two kinds such that

$$\mathbf{f}_{m,n} = -v_{mn}(\mathbf{u}_m - \mathbf{u}_n)$$

is the force reducing \mathbf{u}_m when $\mathbf{u}_m > \mathbf{u}_n$ and vice versa. v_{mn} is called the collision frequency for momentum transfer. The acceleration of m -type particles due to collisions with n -type particles is now:

$$\frac{d\mathbf{u}_m}{dt} = \mathbf{f}_{mn} = -v_{mn}(\mathbf{u}_m - \mathbf{u}_n) \quad (2.29)$$

Since momentum must be conserved during a collision, we have

$$\rho_m \mathbf{f}_{m,n} + \rho_n \mathbf{f}_{n,m} = 0$$

since $\mathbf{f}_{m,n}$ and $\mathbf{f}_{n,m}$ are forces per unit mass, and $\mathbf{f}_{n,m}$ is the force on particles of type n due to the collision with particles of type m . ρ_m and ρ_n are the mass density of species m and n , respectively. Inserting for $\mathbf{f}_{m,n}$ and $\mathbf{f}_{n,m}$ gives:

$$\begin{aligned} \rho_m v_{mn}(\mathbf{u}_m - \mathbf{u}_n) + \rho_n v_{nm}(\mathbf{u}_n - \mathbf{u}_m) &= 0 \\ (\rho_m v_{mn} - \rho_n v_{nm})(\mathbf{u}_m - \mathbf{u}_n) &= 0 \end{aligned}$$

For any \mathbf{u}_m and \mathbf{u}_n therefore

$$\rho_m v_{mn} = \rho_n v_{nm} \quad (2.30)$$

For simplicity we only consider one-dimensional velocities and that there is only one kind of particle type n , then the equation of motion for the m -type particle can be written:

$$\frac{du_m}{u_m - u_n} = -v_{mn} dt$$

and the solution for u_m is:

$$u_m = u_m^0 \exp(-v_{mn}t) + u_n(1 - \exp(-v_{mn}t))$$

if $u_m = u_m^0$ at $t = 0$. The equilibrium solution ($t \rightarrow \infty$) for u_m is:

$$u_m = u_n$$

The characteristic relaxation time is defined as:

$$\tau_{m,n} = \frac{1}{v_{mn}}$$

In the opposite case the velocity of the n -type particle is given from (2.29) by:

$$u_n = u_n^0 \exp(-v_{nm}t) + u_m(1 - \exp(-v_{nm}t))$$

and the relaxation time is:

$$\tau_{n,m} = \frac{1}{v_{nm}} = \frac{\rho_n}{\rho_m v_{mn}} = \frac{\rho_n}{\rho_m} \tau_{mn}$$

when (2.30) is applied. We therefore notice that, if $\rho_m \gg \rho_n$, the n -type particle will reach the equilibrium velocity \mathbf{u}_m much more quickly than the m -type particle will reach its equilibrium velocity \mathbf{u}_n . In such a situation n -type particles will feel the presence of m -type particles much more strongly than the latter type feels the former. This is in simple terms the effect of drag from one kind of gas particle to another.

The mean velocity is defined as:

$$\mathbf{u} = \frac{\rho_m \mathbf{u}_m + \rho_n \mathbf{u}_n}{\rho}$$

where

$$\rho = \rho_m + \rho_n$$

Now, since $d\rho/dt = 0$ we obtain

$$\rho \frac{d\mathbf{u}}{dt} = -(\rho_m v_{mn}(\mathbf{u}_m - \mathbf{u}_n) + \rho_n v_{nm}(\mathbf{u}_n - \mathbf{u}_m)) = 0$$

Therefore, the mean velocity \mathbf{u} is constant and

$$\mathbf{u}(\infty) = \mathbf{u}(t) = \mathbf{u}(0)$$

The collision term being proportional to the relative velocities between each type of particle contributes to a force which tends to drive each individual gas velocity toward a total mean velocity which is constant (i.e., an equalization in velocity takes place).

For the collisional interaction between ions and neutrals in the ionosphere it is of interest to compare the time constants with which the ions approach the neutral motion (τ_{in}) and vice versa (τ_{ni}). Such a comparison is presented for the E-region in [Figure 2.23](#) for different days at an auroral zone station (Tromsø). We notice that while τ_{in} is always less than 10^{-1} s, τ_{ni} is hardly less than 10^4 s. A constant ion velocity acting for several hours is therefore needed in order to bring the neutrals into a motion along with the ions. On the other hand, the ions will almost immediately adjust their velocities to the neutral motion. Therefore, the ion motion can be used as a good tracer of the neutral motion.

2.14 COLLISIONS IN GASES WITH DIFFERENT TEMPERATURES

It is customary to treat the gas of the upper atmosphere as a plasma or fluid, assuming the collisions between individual particles are frequent enough for an MHD description to be valid.

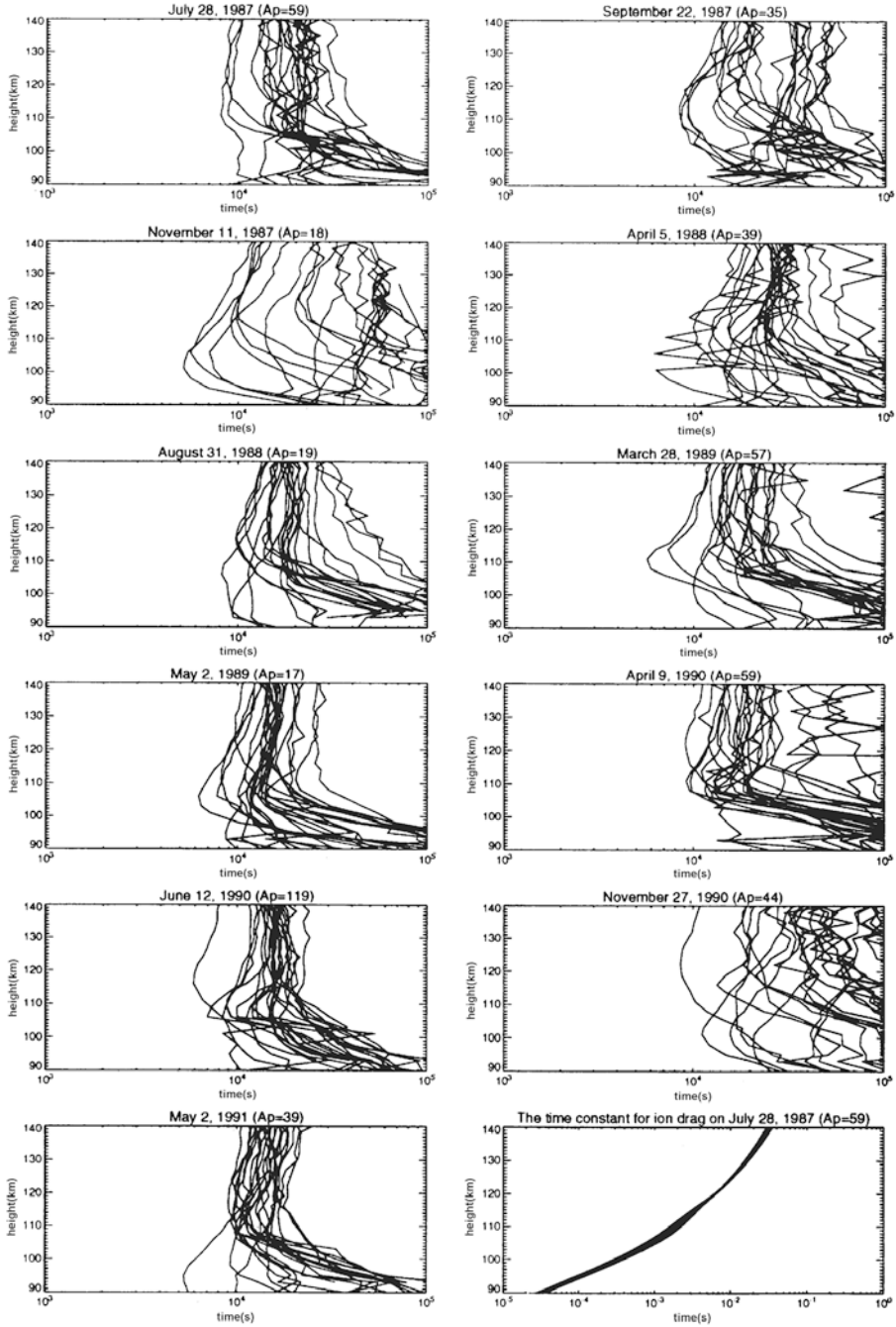


Figure 2.23. A comparison of the time constant τ_{in} for the ions to approach the neutral velocity (the lowest right panel) and τ_{ni} for the neutrals to approach the ion velocity for different days in the E-region above Tromsø (the 11 other panels). (From Nozawa and Brekke, 1995.)

To discuss the collisional interactions between individual kinds of particles m and n in the ionospheric plasma is not a straightforward problem, and it is not the purpose of this book to outline this in detail here.

By performing a statistical analysis where the macroscopic behavior of the plasma is considered to be due to a mean behavior of individual particles, one introduces the distribution function $f_m(\mathbf{r}, \mathbf{u}, t)$. This describes the distribution of particles of kind m having a velocity \mathbf{u} at position \mathbf{r} at time t . The Boltzmann equation describing the variation of this function in space and time can be written as:

$$\frac{\partial f_m}{\partial t} + v_i \frac{\partial f_m}{\partial x_i} + a_i \frac{\partial f_m}{\partial u_i} = \left(\frac{\partial f_m}{\partial t} \right)_c$$

where the index i indicates three individual coordinates, $i = 1, 2, 3$, and the term to the right is the collision term which is crucial for determining the shape of f_m .

By using this equation, however, and forming statistical averages, it is possible to find conservation laws for most parameters related to the behavior of particles of type m .

Boltzmann introduced the following term:

$$\left(\frac{\partial f_m}{\partial t} \right)_c = \sum_n \int (f'_m f'_{n1} - f_m f_{n1}) g b \, db \, d\varepsilon \, d^3 v_1$$

where f_m and f_{n1} are the distribution functions of particles of kind m and n before the collision, respectively, and f'_m and f'_{n1} are the corresponding parameters after the collision, g is the relative velocity between the two kinds of particles, b is the impact parameter, ε is an angle to account for all directions of impact, and $d^3 v_1$ is the velocity space for n -type particles.

For so-called Maxwellian gas particles, where the reaction force between the particles can be expressed as

$$F_R = \frac{\kappa}{r^5}$$

where κ is an arbitrary constant, it can be shown that for such particles in thermodynamic equilibrium the collision term in the energy equation results in a heat transfer rate

$$\frac{dQ_m}{dt} = \frac{\rho_m \nu_{mn}}{m_m + m_n} [3k(T_n - T_m) + m_n(\mathbf{u}_n - \mathbf{u}_m)^2]$$

where k is Boltzmann's constant, T_n and T_m are the temperatures of particles of kind n and m , respectively, and m_n and m_m are their respective masses. This equation shows that as long as the temperatures or the velocities of the two kinds of particles are different, heat transfer between them will occur.

In the ionosphere where the two kinds of particles are neutrals and ions, the last term in the equation above is often referred to as the Joule heating term due to ohmic losses by ionospheric currents. Assuming one type of ions (i) and one

type of neutrals (n) only, we obtain for the heating rate:

$$\frac{dQ_i}{dt} = \frac{\rho_i \nu_{in}}{m_i + m_n} [3k(T_n - T_i) + m_n(\mathbf{u}_n - \mathbf{v}_i)^2] \quad (2.31)$$

where we have introduced \mathbf{v}_i and \mathbf{u}_n as the ion and neutral velocities, respectively.

2.15 DRAG EFFECTS

Let us consider the ionosphere where we have one kind of ion and one kind of neutral with velocities \mathbf{v}_i and \mathbf{u}_n , respectively. Assume an initial situation where $\mathbf{u}_n = 0$ and that an electric field \mathbf{E}_\perp perpendicular to \mathbf{B} induces an ion velocity \mathbf{v}_{i0} according to the “frozen-in” concept:

$$\mathbf{v}_{i0} = \mathbf{E}_\perp \times \mathbf{B} / B^2$$

If \mathbf{E}_\perp is directed eastward (Figure 2.24(a)), then v_{i0} will be upward and northward in the magnetic meridional plane. There will then be a horizontal ion velocity in this plane. Since the neutral gas is considered to be in hydrostatic equilibrium, we can neglect any motion of the neutrals in the vertical direction. The horizontal ion velocity component will then drag the neutrals along after some time. Since the neutrals effectively drag the ions with them, the ions will also obtain a component $\mathbf{v}_{i\parallel}$ parallel to the magnetic field. A stationary state will be obtained when the ions and the neutrals are moving horizontally at the same speed. This occurs when

$$u_n = \frac{v_{i0}}{\sin I} = \frac{1}{\sin I} \frac{E}{B}$$

where I is the inclination angle of \mathbf{B} . The time constant for this to happen in the ionosphere is very long due to the small ρ_i/ρ_n ratio. Assume instead the ions are initially at rest and that a neutral wind \mathbf{u}_{n0} is blowing horizontally in the negative y -direction (south) in the northern hemisphere (Figure 2.24(b)). The component of the wind parallel to the magnetic field will drag the ions until they reach a steady-state velocity \mathbf{v}_i along the field which is given by

$$v_i = u_{n0} \cos I$$

The ions therefore attain a vertical velocity given by

$$v_{iV} = u_{n0} \cos I \sin I$$

and a horizontal velocity

$$v_{iH} = u_{n0} \cos^2 I$$

Let us again assume that $\mathbf{u}_n = 0$ initially and that the plasma is diffusing downward at a velocity v_{iD} (Figure 2.24(c)) due to gravity and pressure gradients. Since a magnetic field is present, ions are forced to follow field lines. The ion motion will therefore attain a horizontal component given by:

$$v_{iH} = v_{iD} \cos I$$

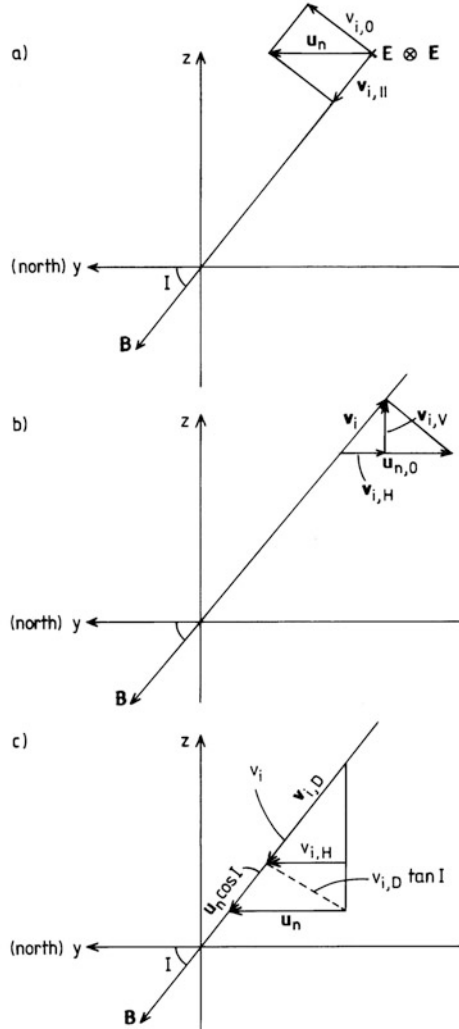


Figure 2.24. Diagrams illustrating the different drag effects taking place between the neutral and the ionized gas species in the upper atmosphere. (a) The neutral gas is initially at rest. An electric field perpendicular to \mathbf{B} is associated with an ion drift $\mathbf{v}_{i,0}$. Since the neutrals are restricted to moving mainly horizontally, there will be a horizontal neutral velocity \mathbf{u}_n . This neutral velocity will drag the ions along the \mathbf{B} -field, and the ions will obtain a velocity component $\mathbf{v}_{i,||}$ parallel to \mathbf{B} . A steady-state situation occurs when the ions and the neutrals are moving horizontally at the same speed. (b) The ions are initially at rest and the neutral gas moves horizontally at velocity $\mathbf{u}_{n,0}$. The component of the neutral velocity along \mathbf{B} drags the ions along until they reach a steady-state velocity \mathbf{v}_i equal to this component. (c) The neutral gas is initially at rest while the plasma diffuses downward along \mathbf{B} at a velocity $\mathbf{v}_{i,D}$. The horizontal component of this velocity will drag the neutrals along until they reach a velocity \mathbf{u}_n . This horizontal neutral motion will again drag the ions down along the \mathbf{B} -field, and a steady state occurs when the horizontal neutral and ion velocities are equal.

This will drag the neutrals along until they eventually obtain a horizontal velocity u_n . Then the neutrals will also drag the ions along the B -field by the component $u_n \cos I$. Equilibrium is obtained when the ions and neutrals move horizontally at the same speed. This happens when

$$(v_{iD} + u_n \cos I) \cos I = u_n$$

$$u_n = \frac{v_{iD} \cos I}{\sin^2 I}$$

and then the plasma velocity along the field becomes:

$$v_i = v_{iD} / \sin^2 I$$

2.16 THERMOSPHERIC NEUTRAL WINDS

Atmospheric drag on satellites has been extensively used to deduce the temperature distribution in the upper thermosphere, especially at the thermopause. [Figure 2.25](#) is a representation of the inferred isotherms at the thermopause on the basis of a large number of satellite passes. The temperature distribution is rather symmetric around the equator but is shifted about one hour to the east of the

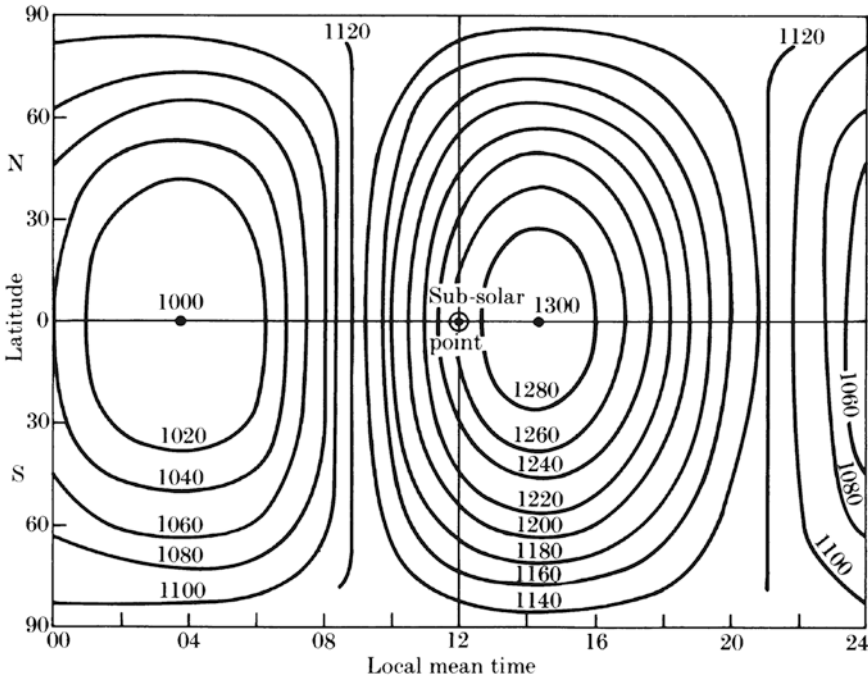


Figure 2.25. The inferred isotherms at the thermopause. The numbers labeled on the contours are in kelvins. (From Jacchia, 1965.)

subsolar point, probably due to sluggishness in the neutral gas. For this special diagram a maximum temperature of about 1,300 K is observed at the equator at about 14:00 LT. This maximum temperature, however, is sensitive to solar cycle variations and to magnetospheric disturbances. In fact, it does appear that the temperature at the thermopause is more sensitive to magnetic disturbances than to variations in solar EUV flux.

The daily global temperature distribution as shown in Figure 2.25 leads to a daytime expansion of the atmosphere which is called the “diurnal bulge”. The horizontal pressure gradients around this “diurnal bulge” provide the driving force for thermospheric winds. From this type of temperature distribution it is then possible to derive the large-scale pressure gradients and from those again to calculate the resulting neutral wind when applying an appropriate equation of motion for the neutrals. Figure 2.26 gives an example of such calculations where we notice that the velocities are directed from the hot dayside across the pole to the nightside (i.e., the wind is very close to being perpendicular to the isotherms). The wind speeds are of the order of 40 m/s.

Let us for simplicity neglect all other terms than the pressure gradient force and \mathbf{f} in the equation of motion for the neutral gas (2.25). Then for a steady-state solution of the horizontal winds (as Figure 2.26 represents):

$$\mathbf{f} = \frac{1}{\rho} \nabla p$$

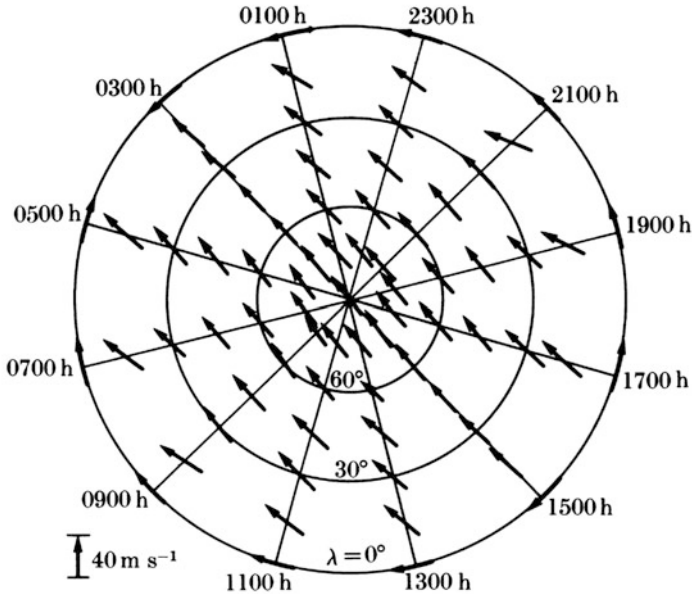


Figure 2.26. The inferred wind system at an altitude of 300 km based on a temperature distribution of the thermopause similar to the one shown in Figure 2.25. (From Kohl and King, 1967.)

If now \mathbf{f} is due only to collisions ($-\nu_{ni}(\mathbf{u}_n - \mathbf{v}_i)$) between the neutral gas and the ions in the thermosphere and assuming that the ions are stationary, then:

$$u_n = -\frac{1}{\rho \cdot \nu_{ni}} \nabla p = -\frac{k}{m\nu_{ni}} \nabla T$$

where we have assumed an ideal gas and neglected horizontal variations in the neutral density. ν_{ni} is the neutral-ion collision frequency. In this simplified situation we therefore find that the neutral wind should blow down the temperature gradients (i.e., perpendicularly to the isotherms shown in [Figure 2.25](#)). We also notice, however, that only for very high collision frequencies can it be legitimate to neglect all other terms in the equation of motion except the pressure force and the collision term. For smaller collision frequencies the situation will be more complex.

A more realistic treatment makes the equation of motion for the neutrals far more difficult to solve, especially when we notice that the ions are not at all stationary at times at high latitudes when they are acted on by electric fields propagating from the magnetosphere. Furthermore, neutral air motion at one height can carry the ions along, which will in turn set up polarization fields that can propagate to other heights and other latitudes along magnetic field lines where they can act on the ion motion. The collisions between the ions and the neutrals will always be present, forcing the different species to drag each other.

Returning again to the equation of motion (2.25) and dividing the force term \mathbf{f} up into a potential term, a viscosity term, and a collision term, we can write:

$$\frac{\partial \mathbf{u}_n}{\partial t} = -(\mathbf{u}_n \cdot \nabla) \mathbf{u}_n - 2\mathbf{\Omega} \times \mathbf{u}_n + \mathbf{g} - \frac{1}{\rho} \nabla p - \nabla \psi + \frac{\mu}{\rho} \nabla^2 \mathbf{u}_n - \nu_{ni}(\mathbf{u}_n - \mathbf{v}_i) \quad (2.32)$$

where ψ is a potential due to the centrifugal force and tides, μ the coefficient of viscosity, and \mathbf{v}_i the ion velocity. In order to get a better understanding of the neutral wind behavior we need to know more about the different terms. Especially since we observe that the velocity of the ion gas enters the equation of motion for the neutrals, the equation of motion for the ions should also be solved simultaneously to give a self-consistent picture. Let us therefore introduce the equation of motion for ions:

$$m_i \frac{\partial \mathbf{v}_i}{\partial t} = -m_i(\mathbf{v}_i \cdot \nabla) \mathbf{v}_i + q\mathbf{E} + q\mathbf{v}_i \times \mathbf{B} - m_i\nu_{in}(\mathbf{v}_i - \mathbf{u}_n) \quad (2.33)$$

where m_i is the ion mass, q the ion charge, and \mathbf{E} the electric field. We have neglected the Coriolis force, gravity, potential, and pressure forces together with viscosity since these are considered to be small in the thermosphere compared with the electric field, Lorentz force, and collision terms. We now observe that since the electric field and Lorentz force enter into the equation of motion for the ions, these may also affect the motion of the neutrals through the collision term between ions and neutrals. In a situation where \mathbf{E} is very large, the ion velocity may dominate and the neutrals act as a drag on ions. In the opposite case when the \mathbf{E} -field is negligible, the ions may act as a drag on neutrals. Since the \mathbf{E} -field is

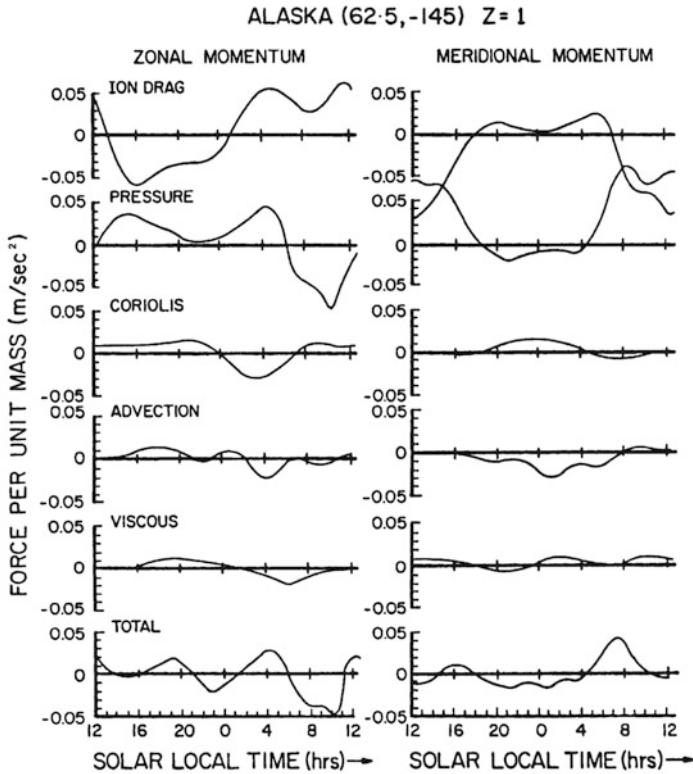


Figure 2.27. Analysis of forces for the neutral gas over the Alaska station (62.5° N , -145° E) calculated under conditions corresponding to December 4, 1981, for the F-region height at about 300 km. (From Killeen and Roble, 1986.)

so variable, especially at high latitudes, it is realized that the neutral gas motion can be a strongly modified and dynamic feature of the thermosphere.

Since there are so many dynamic parameters affecting the neutral gas motion, it is an almost insurmountable problem to obtain a comprehensive view of the situation. We have to make some assumptions and hope that the results we derive have a validity general enough that we can use them as a rule of thumb.

In [Figure 2.27](#) calculations obtained for a high-latitude station (Chatanika, Alaska, 62.5° N , -145° E) pertinent to different terms in the equation of motion for the neutrals are illustrated. The potential term $\nabla\psi$ in equation (2.32), however, is neglected.

We notice from [Figure 2.27](#), which applies for an altitude close to 300 km, that the ion drag and the pressure terms are dominant for both meridional and zonal components.

In the auroral zone and high latitudes where the ion velocity may become much larger than the neutral velocity, it is not legitimate to neglect the ion velocity in the collision term in equation (2.32). In a steady state to a first approximation

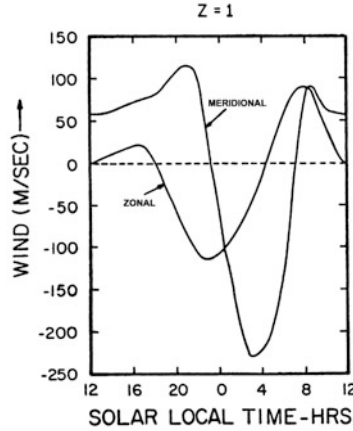


Figure 2.28. F-region neutral wind predictions for a station in Alaska corresponding to conditions as of December 4, 1981, at F-region heights (300 km). Of particular interest is the strong equatorward surge in the meridional component after midnight: a common feature observed at this station is apparently a consequence of the pressure and ion drag terms acting together on the neutral gas. (From Killeen and Roble, 1986.)

the neutral wind will therefore be:

$$\mathbf{u}_n = -\frac{1}{\rho\nu_{ni}}\nabla p + \mathbf{v}_i$$

This implies that the ion velocity can have a strong effect on the neutral velocity. This is illustrated in [Figure 2.28](#) where a large equatorward surge in the neutral velocity occurs at night-time having a maximum of close to 200 m/s. This is apparently related to an enhancing effect of the pressure term and the ion drag term in the mobility equation. They both happen to force the neutrals in the same direction at this time over Alaska. A southward motion would be expected from the pressure gradients alone, but the ion motion, which for this particular day, December 4, 1981, was forced by a cross-polar cap electric field corresponding to about 60 kV, enhanced the equatorward motion in the morning hours.

At higher latitudes, within the polar cap where it is possible to observe the Doppler-shifted O I (6,300 Å) line throughout a 24-hour period in midwinter, the neutral wind is found to be nearly cross-polar from day to night ([Figure 2.29](#)). In this diagram the circle marks the latitude of observation (Longyearbyen, Svalbard, 78° N), and the center of the circle is the geographic north pole. The diagram does not represent a snapshot of the wind vectors since the observations are collected over a 24-hour period. Under the assumption, however, that the wind pattern does not change during this period of observations, it can be interpreted as an instantaneous pattern.

In [Figure 2.30\(a\)](#) more detailed model calculations of the global F-region neutral wind circulation field are demonstrated as a function of longitude and latitude toward a background of isothermal contours. This can be compared with

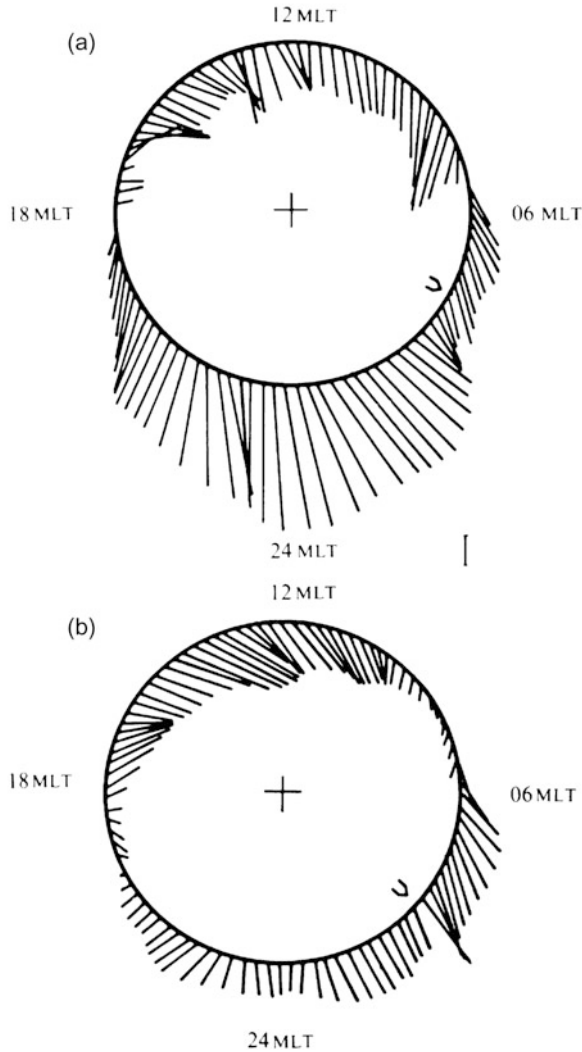


Figure 2.29. Neutral wind patterns in the polar thermosphere obtained for two days, January 21 and 29, 1979. The circle and the center represent the latitude of Longyearbyen, Svalbard (78° N) and the geographic north pole, respectively. An arrow pointing toward the center is a northward wind and tangentially toward the right from north is eastward. The scale bar corresponds to a wind velocity of 100 m/s. (From Smith and Sweeney, 1980.)

the one shown in [Figure 2.26](#). In this model ([Figure 2.30\(a\)](#)) there is no potential drop across the polar cap such that ions act as a drag on neutrals. Again we notice that the main wind field is perpendicular to the isotherms from the hot subsolar point at about 16:00 LT toward the cooler nightside. The cross-polar cap neutral wind is rather outstanding, reaching velocities of the order of 100 m/s.

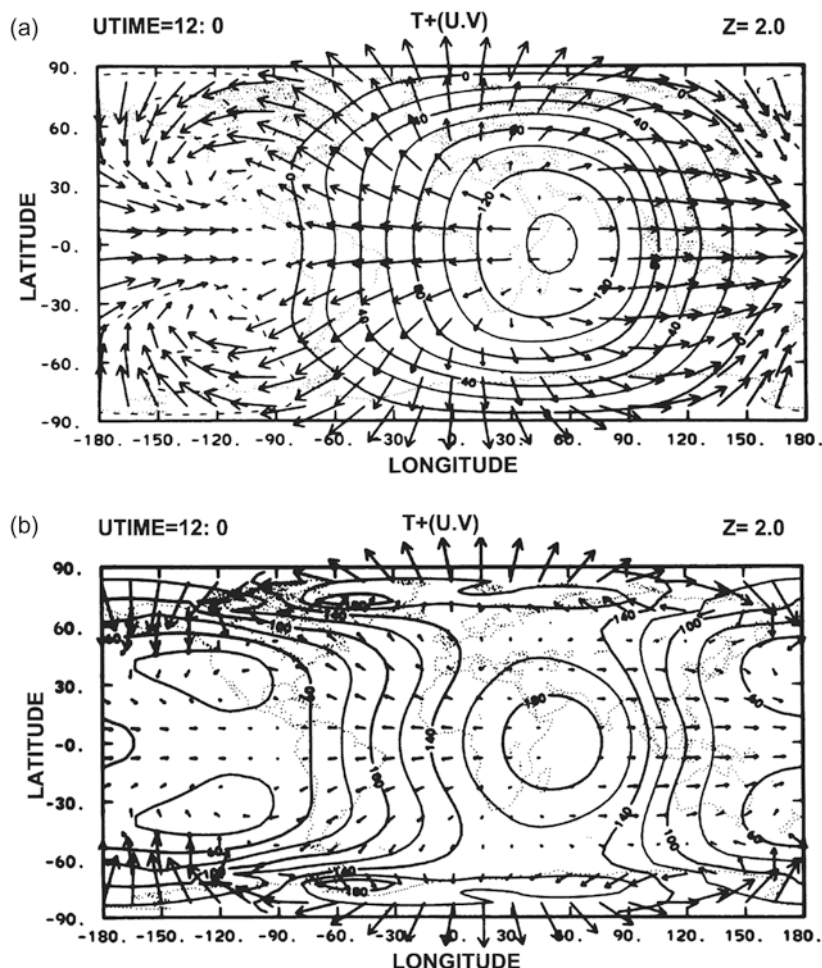


Figure 2.30. (a) Calculated global circulation and temperatures along a constant pressure surface corresponding to about 300 km for the case of solar heating as the only driving force mechanism. The contours describe the temperature perturbation in K and the arrows give wind directions. The length of the arrows gives the wind speed with a maximum of 100 m/s. (b) The same as in (a) except that a magnetospheric convection source with cross-tail potential corresponding to 60 kV is included. The wind speed represented by the length of arrows now corresponds to 336 m/s. (From Dickinson *et al.*, 1984.)

When, however, a cross-polar cap potential of about 60 kV is applied (Figure 2.30(b)), the wind field as well as the temperature distribution changes character; the latter is related to local heating due to enhanced collisions between the neutrals and ions (Joule heating). The velocities across the polar region are strongly enhanced (notice the change in scales by a factor of more than 3 on the velocity arrows). At night-time the high-latitude velocities are more strongly equatorward related to the surge, as noticed already in relation to Figure 2.28. In

the daytime, however, at middle latitudes the velocities are strongly reduced and the zonal component is reversed from eastward to westward. These effects are due to enhanced Joule heating at high latitudes caused by strong currents in the auroral zone.

That electromagnetic disturbances at high latitudes can have a significant effect at thermospheric heights is illustrated more clearly in [Figure 2.31](#). In panel (a) the meridional circulation under quiet conditions is mainly forced by solar heating which produces a large cell with warm air rising at the equator, flowing towards the poles, and sinking down again to lower heights. Above the polar regions ($>70^\circ$ latitude), however, a small cell with the opposite flow direction is set up above 300 km altitude due to heat influx from the magnetosphere outside the plasmapause. In panel (b), however, in which a large magnetic storm takes place, the contrary cell expands in altitude (down to 120 km) as well as in latitude (down to the equator around 200 km of altitude). Air rich in molecular constituents rises in the thermosphere above the high-latitude regions and is being brought at high altitude toward the equator where the air descends to about 150 km. Ions with high velocities are observed flowing outward from the thermosphere along magnetic field lines during such stormy events.

2.17 E-REGION WINDS

By now moving down in altitude to study E-region winds, it is again useful to compare the different terms in the equation of motion (2.26). In [Figure 2.32](#) the outcome of such a comparison for the same high-latitude station as shown in [Figure 2.27](#) is presented.

Contrary to the F-region situation where the pressure and ion drag term appeared to be dominant forcing mechanisms to the neutral wind, it is the pressure and Coriolis term that rule over the E-region neutral air motion. A global model calculation of the E-region neutral wind at about 120 km of altitude is illustrated in [Figure 2.33\(a\)](#) against isothermal contours. It is noticed that in contrast to F-region winds which are mainly directed perpendicularly to the isotherms, the E-region neutral air motion more closely follows these contour lines. A geostrophic component is therefore present in E-region neutral winds. E-region wind speeds are also only a third of F-region speeds on average. A 60 kV cross-polar cap potential is enforced on the ion motion for the wind data shown in [Figure 2.33\(b\)](#). The high-latitude winds are now predominantly eastward and the cross-polar cap motion is reduced. At low latitudes, however, there do not appear to be marked changes in the E-region wind field.

2.18 OBSERVATIONS OF E-REGION NEUTRAL WINDS

Due to the strong coupling between neutrals and ions in the E-region, observations of the ion motion can sometimes be used as a tracer for the neutral motion.

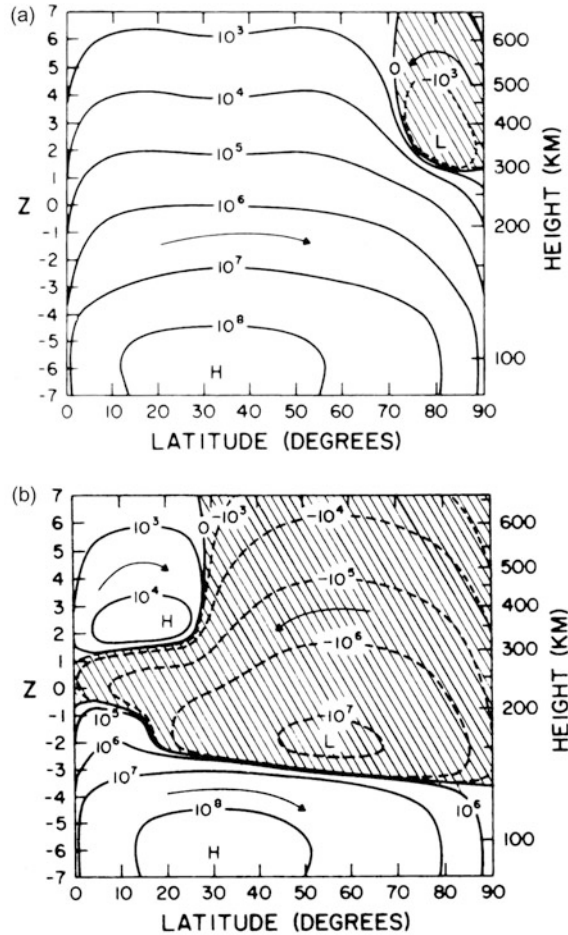


Figure 2.31. Calculated contours of a mass flow stream function. The numbers on the contours are in g/s. The difference between the contour values gives the global flux mass between the two contours. (a) For solar heating as the only driving source. (b) For solar heating, Joule heating and momentum source also included. (From Dickinson *et al.*, 1975.)

Let us now consider the equation of motion for the ions (2.33). In the steady state when $dv_i/dt = 0$, we can solve for neutral velocity in a simple manner:

$$\mathbf{u}_n = \mathbf{v}_i - \frac{q}{m_i v_{i,n}} \mathbf{v}_i \times \mathbf{B} - \frac{q}{m_i v_{i,n}} \mathbf{E} \quad (2.34)$$

At high latitude where the magnetic field is almost vertical, this equation applies to the horizontal component of \mathbf{u}_n while the vertical component is assumed equal to the ion motion along the magnetic field line. We notice that when v_{in} is very large, the neutral velocity is equal to the ion velocity. Observing the ion motion by some radio or radar technique therefore allows for deriving the neutral motion

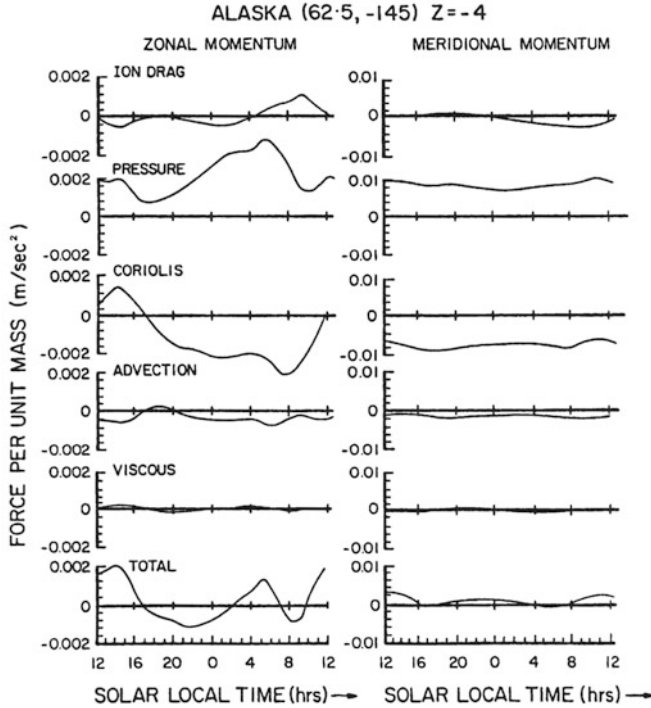


Figure 2.32. Similar to the data shown in Figure 2.27 but applied at 120 km approximately. (From Killeen and Roble, 1986.)

in a rather direct manner. For smaller values of ν_{in} the complete coupling between ions and neutrals as given by (2.34) has to be accounted for in order to derive \mathbf{u}_n from measurements of \mathbf{v}_i . By means of an incoherent scatter radar such as EISCAT close to Tromsø, Norway (70° N) one can obtain almost simultaneous observations of E- and F-region velocities. In the F-region (300 km) where the collision term will be negligible to the ion motion compared with the E-field and Lorentz force term, the electric field can be derived for a steady-state solution (1.29):

$$\mathbf{E} = -\mathbf{v}_i^F \times \mathbf{B}$$

where \mathbf{v}_i^F is the F-region ion velocity observed simultaneously with the E-region ion velocity. The neutral wind in the E-region can then be derived with an appropriate choice of collision frequency model.

Figure 2.34 illustrates neutral wind (x, y, z) components in the geographical frame of reference as a function of time at several E-region heights for quiet days ($A_p \leq 16$) in the four seasons. From such time series the mean velocity components as well as the average 24-, 12-, 8-, and 6-hour tidal components can be derived for each of the six heights. This has been carried out for all four seasons and the results are presented in Figure 2.35. The most outstanding feature of these

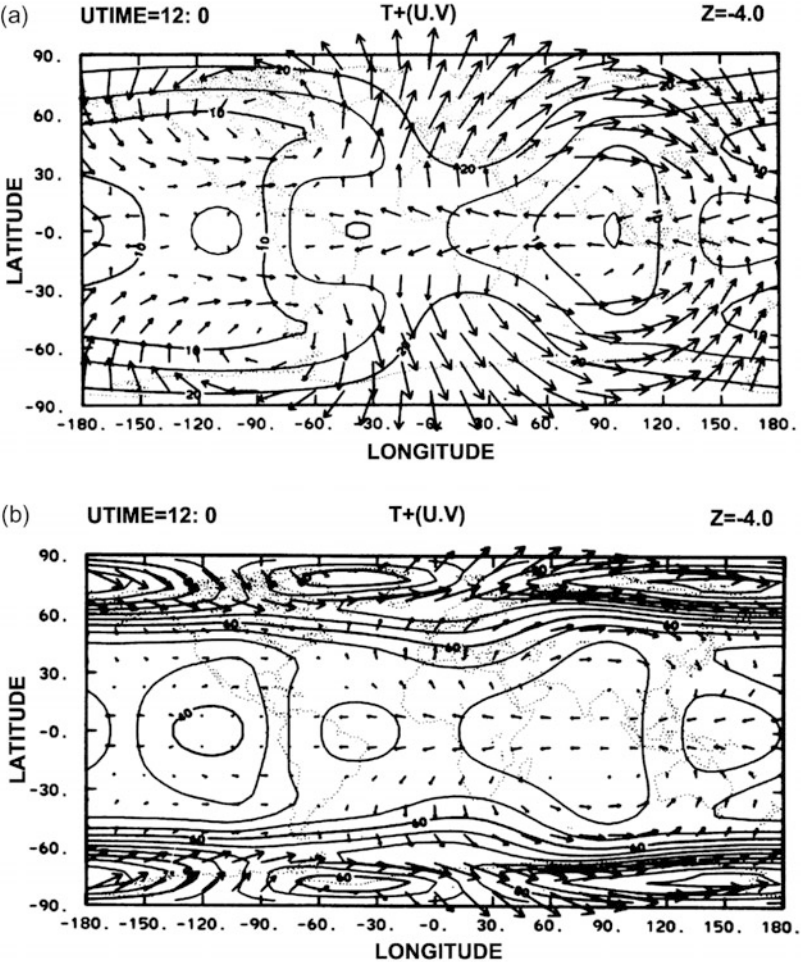


Figure 2.33. Same as for [Figure 2.30](#) except that the constant pressure level corresponds to close to 120 km. (a) The maximum wind speed corresponds to 32 m/s. (b) The maximum wind speed corresponds to 79 m/s. (From Dickinson *et al.*, 1984.)

components is the strong mean eastward wind between 90 and 120 km having a maximum at about 110 km of 60 m/s in summer and 20 m/s in winter. The very low mean northward and vertical wind components in the same height region are also noticeable; these components are relatively less influenced by change of season.

The eastward component of the diurnal tide increases gradually by height and reaches an amplitude close to 100 m/s above 120 km. The northward component of this tide is fairly independent of height. For the other horizontal tidal components no systematic height dependence is found. In the vertical component, however, all tidal components except the 6-hour tide have a minimum amplitude at the height

region of the strong mean eastward wind. In [Figure 2.36](#) wind components presented as a function of time for the six E-region heights for quiet autumn days in [Figure 2.34](#) are shown as horizontal clock dial plots. We notice the outstanding daytime poleward wind at the four lower heights 96–117 km. Clearly, there are large variations by height in the neutral wind in the auroral E-region.

It is generally believed, in spite of the long time constants involved (as shown in [Figure 2.23](#)), that the E-region neutral velocities will be modified during strong auroral disturbances at the higher latitudes.

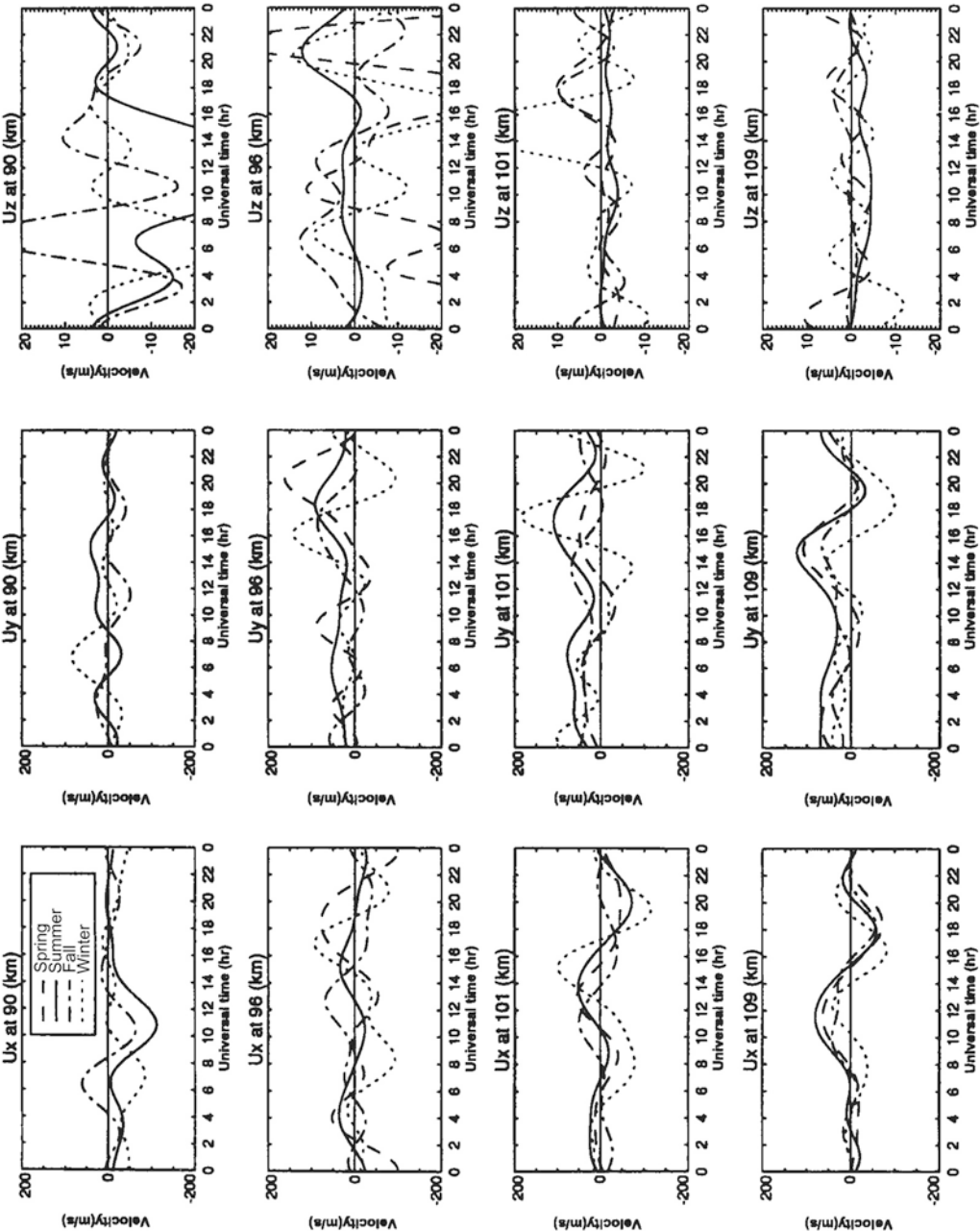
A similar averaging process of the average neutral wind at different E-region heights has been performed on data obtained by EISCAT under disturbed conditions ($A_p > 16$). The mean velocity components as well as the tidal components are shown as a function of height in [Figure 2.37](#). Data obtained from 11 disturbed days are compared with corresponding data from 24 quiet days ($A_p \leq 16$). We notice that the strong eastward mean velocity is rather unaffected by the condition of disturbance, and is more dependent on season (as shown in [Figure 2.35](#)). An outstanding feature in the auroral E-region is therefore an eastward neutral jet stream or superrotation. The most outstanding difference between quiet and disturbed days appears to be the enhancement of the eastward diurnal tide above 110 km altitude.

By the EISCAT Svalbard Radar (ESR) it is also possible to derive the E-region neutral wind at polar latitudes. A comparison of the height profiles of the mean wind and diurnal and semidiurnal tides is shown in [Figure 2.38](#) for observations in Tromsø and Longyearbyen, Svalbard (78.1°N , 15.3°E). It is noticed that the behavior of the different components is rather similar except that the mean eastward wind in Tromsø is weaker than in the polar cap latitude.

To study the importance of the electric field on the neutral wind at different heights, [Figure 2.39](#) shows a correlation analysis of the horizontal neutral wind components and the electric field at different altitudes as derived from Tromsø and Svalbard. It is noticed that the correlation coefficient is very low (~ 0) below 110 km for all components and that the neutral wind appears to be less influenced by the E-field above 110 km in Longyearbyen than in Tromsø. The ion drag appears to be less efficient at higher latitudes. The eastward component of the neutral wind in Tromsø appears almost in antiphase with the electric field above 120 km while the northward component has a maximum correlation for both places at about 115 km.

2.19 VERTICAL MOTION

It is of special interest to study vertical winds, although these are usually very small compared with horizontal winds and also difficult to measure. They are, however, important as they play a significant role in the vertical transport of momentum and kinetic energy, and also of gravity potential energy. Furthermore, vertical winds control to a large extent the vertical distribution of the different constituents as we have seen in relation to diffusion. Let us assume that there are



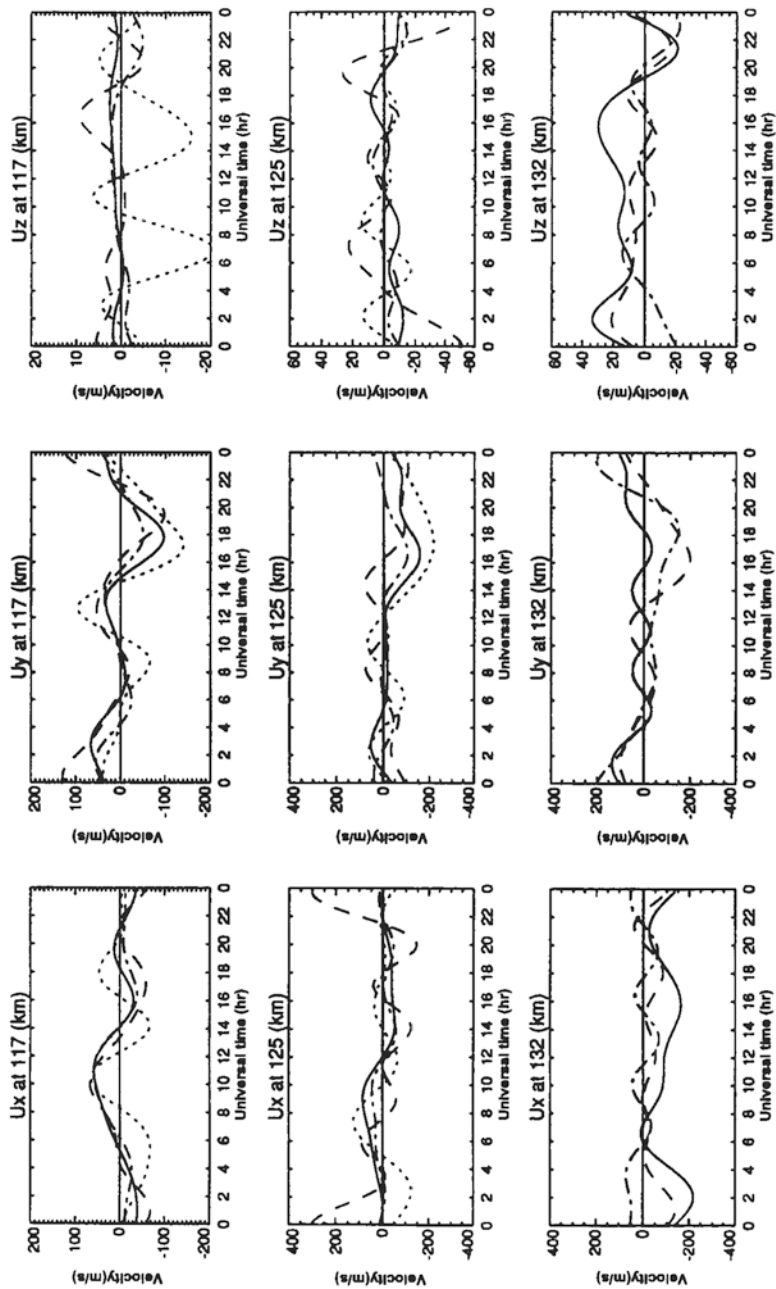
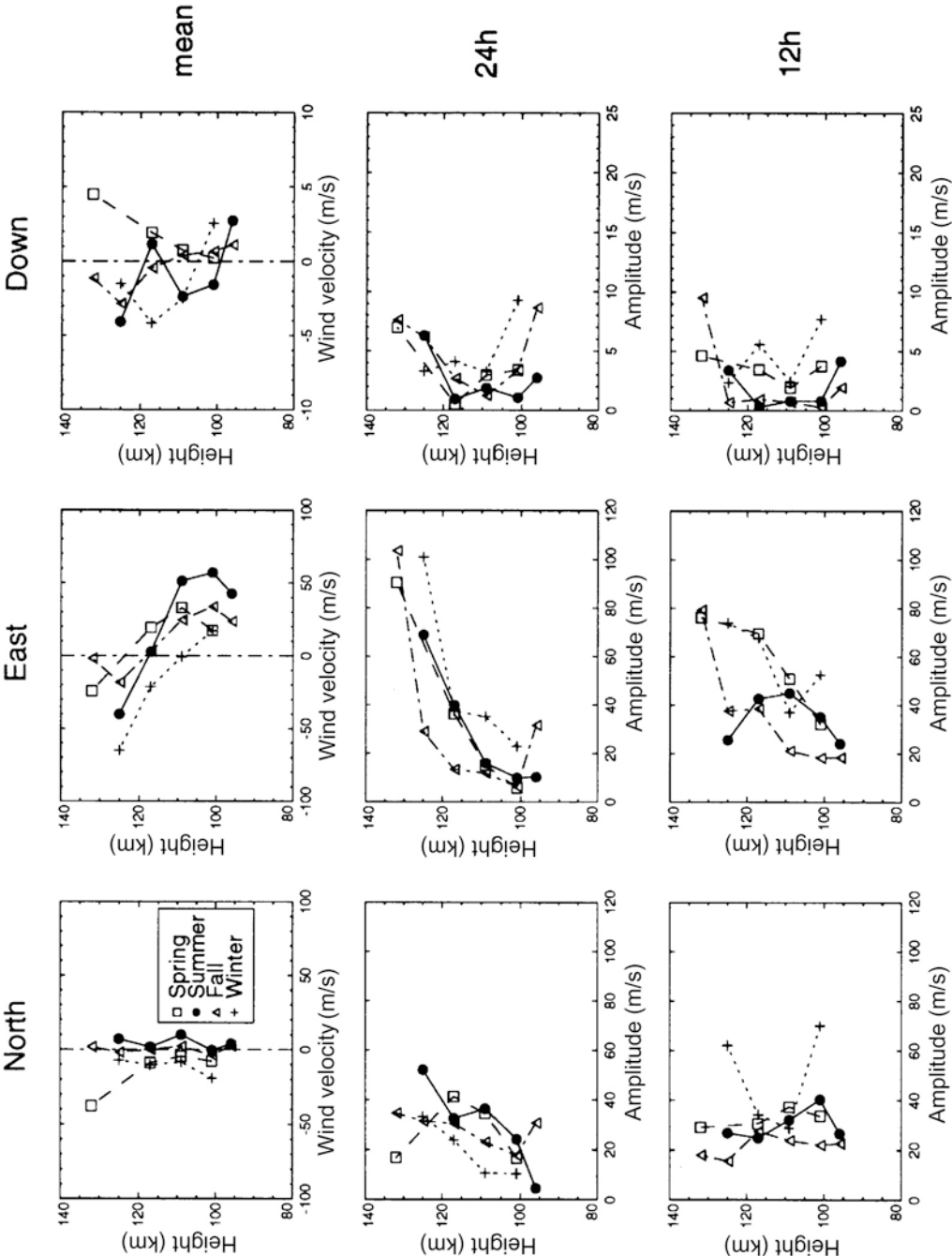


Figure 2.34. The average neutral wind components derived by the EISCAT incoherent scatter radar at Tromsø (69.66° N, 18.94° E) at seven E-region heights for quiet days ($A_p \leq 16$) in the four seasons. These average wind components are derived by adding the mean wind components together with the 24-, 12-, 8-, and 6-hour tidal components with appropriate phases. (Courtesy Nozawa, 1994.)



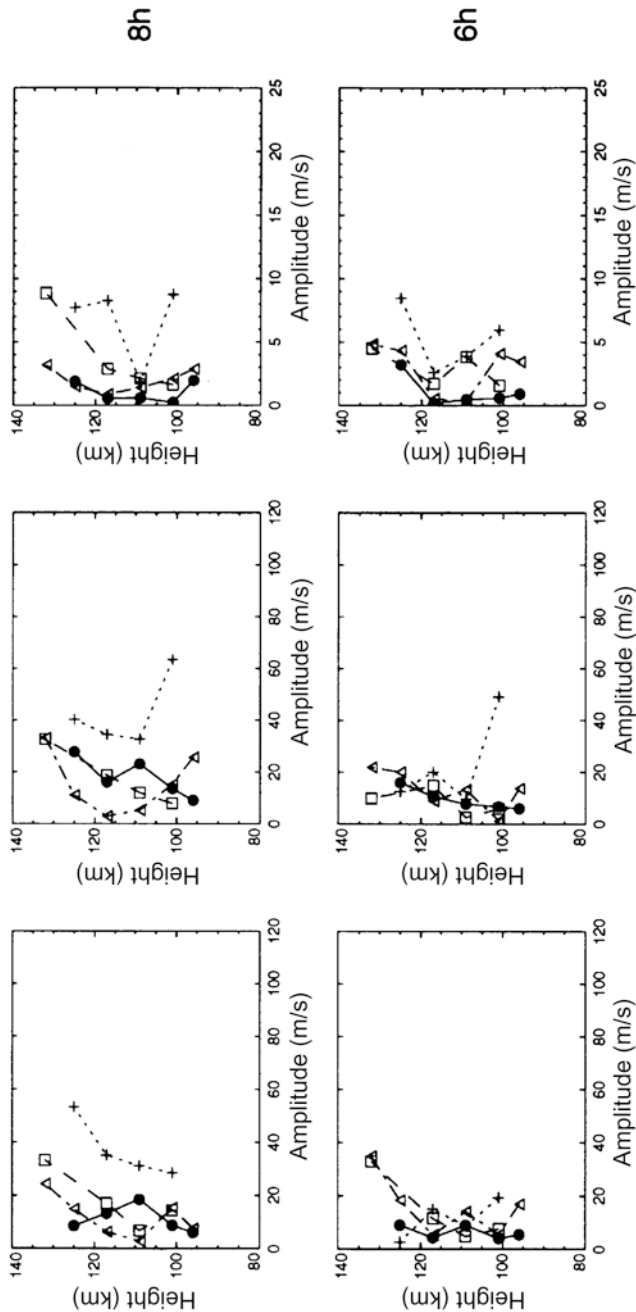


Figure 2.35. (Upper row of panels) The mean components as a function of height for the four seasons. (Four lower rows of panels) The 24-, 12-, 8-, and 6-hour tidal components as a function of height for the four seasons. (From Brekke *et al.*, 1994.)

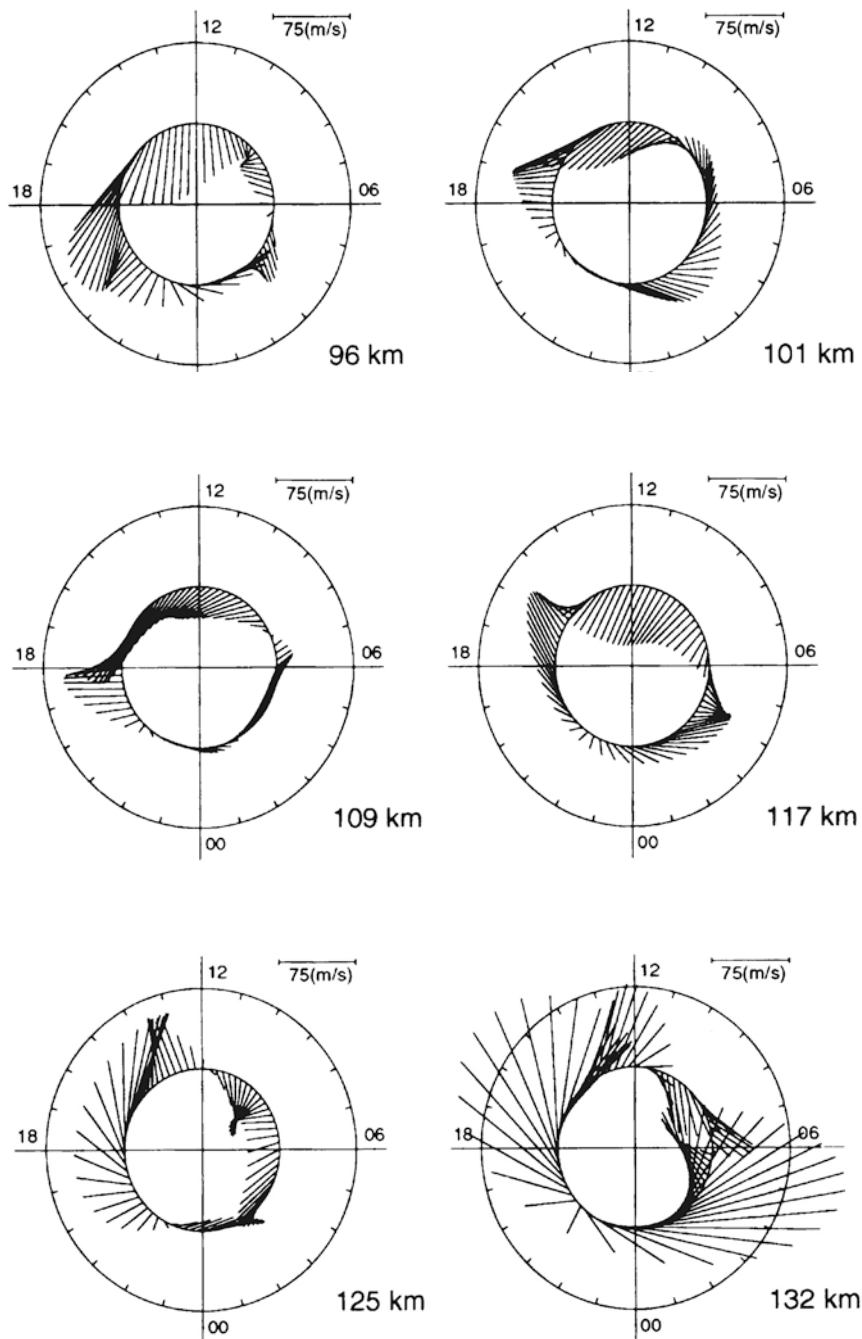


Figure 2.36. The average horizontal neutral wind velocity vectors at six different E-region heights for the average quiet autumn day. These vectors are obtained by adding together the appropriate north and east components in [Figure 2.34](#). (From Brekke *et al.*, 1994.)

no horizontal gradients in density but that the atmosphere is vertically stratified ($\partial/\partial x = \partial/\partial y = 0$).

For a quasi-steady state ($\partial/\partial t = 0$) we derive from the continuity equation

$$\left. \begin{aligned} \frac{d\rho}{dt} + \rho \nabla \cdot \mathbf{u} &= 0 \\ \frac{\partial \rho}{\partial t} + (\mathbf{u} \cdot \nabla) \rho + \rho \nabla \cdot \mathbf{u} &= 0 \\ (\mathbf{u} \cdot \nabla) \rho + \rho \nabla \cdot \mathbf{u} &= 0 \end{aligned} \right\} \quad (2.35)$$

and

$$w \frac{\partial \rho}{\partial z} + \rho \nabla \cdot \mathbf{u} = 0$$

where we have used $\mathbf{u} = (u, v, w)$. By multiplying by p and dividing by ρ we get

$$p \nabla \cdot \mathbf{u} = - \frac{p}{\rho} \frac{\partial \rho}{\partial z} w \quad (2.36)$$

From the equation of state for an ideal gas

$$p = \rho R T \quad (2.37)$$

where $R = 8.3 \text{ J/mol K}$ is the individual gas constant, we form

$$\frac{\partial p}{\partial z} = R \left(\rho \frac{\partial T}{\partial z} + T \frac{\partial \rho}{\partial z} \right)$$

and solving for $\partial \rho / \partial z$ gives:

$$\frac{\partial \rho}{\partial z} = \frac{1}{T} \left(\frac{1}{R} \frac{\partial p}{\partial z} - \rho \frac{\partial T}{\partial z} \right)$$

By inserting this into (2.36) we have

$$p \nabla \cdot \mathbf{u} = - \frac{p}{\rho} \frac{1}{T} \left(\frac{1}{R} \frac{\partial p}{\partial z} - \rho \frac{\partial T}{\partial z} \right) w = - \left(\frac{\partial p}{\partial z} - \frac{p}{T} \frac{\partial T}{\partial z} \right) w$$

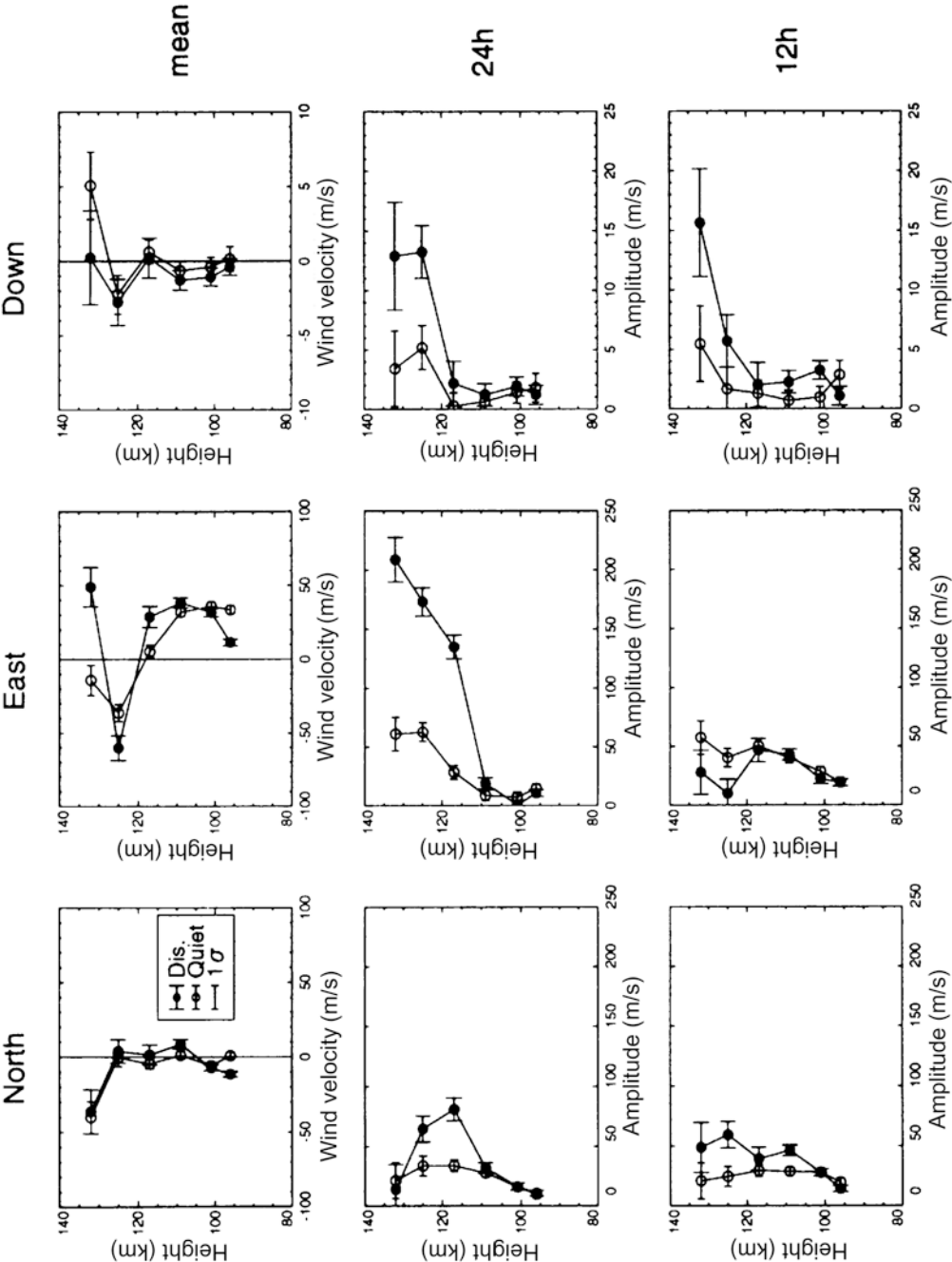
The vertical velocity is now given by

$$w = - \frac{p \nabla \cdot \mathbf{u}}{\frac{\partial p}{\partial z} - \frac{p}{T} \frac{\partial T}{\partial z}}$$

By introducing the partial derivative $\partial T / \partial p$ and the barometric law (2.5) we have:

$$w = \frac{p \nabla \cdot \mathbf{u}}{g \rho \left(1 - \frac{p}{T} \frac{\partial T}{\partial p} \right)} \quad (2.38)$$

The vertical velocity is now expressed by the divergence of \mathbf{u} and the variation in temperature by pressure. By introducing the scale height from (2.6) into (2.38), we



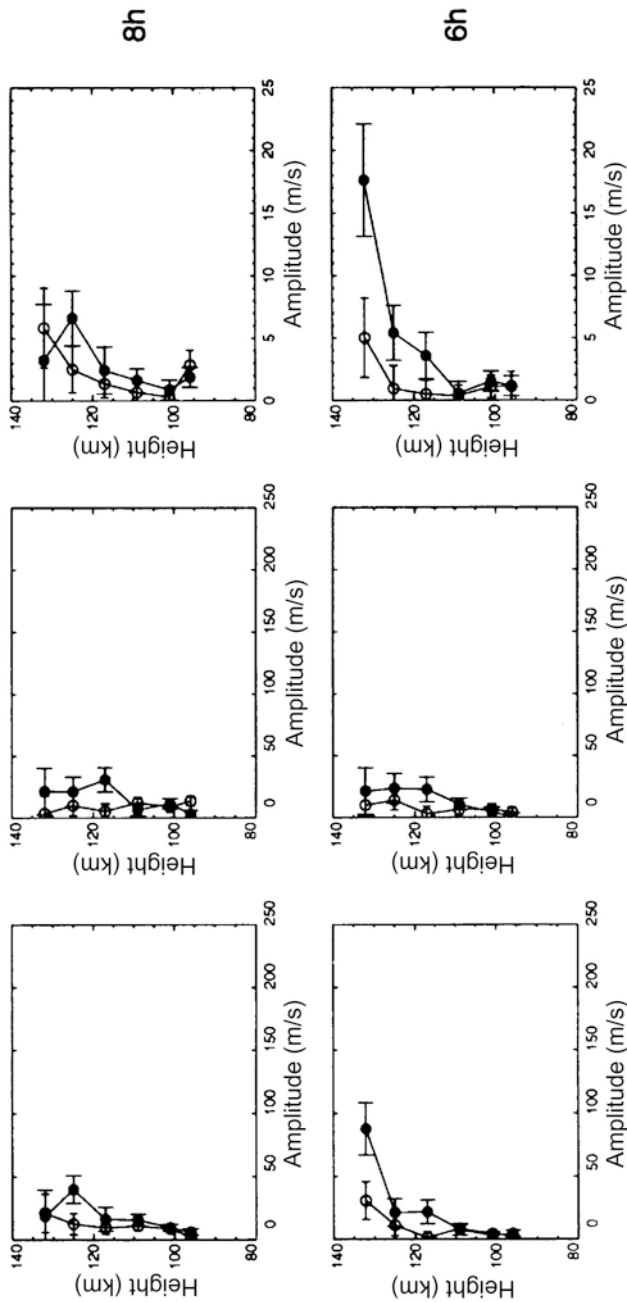
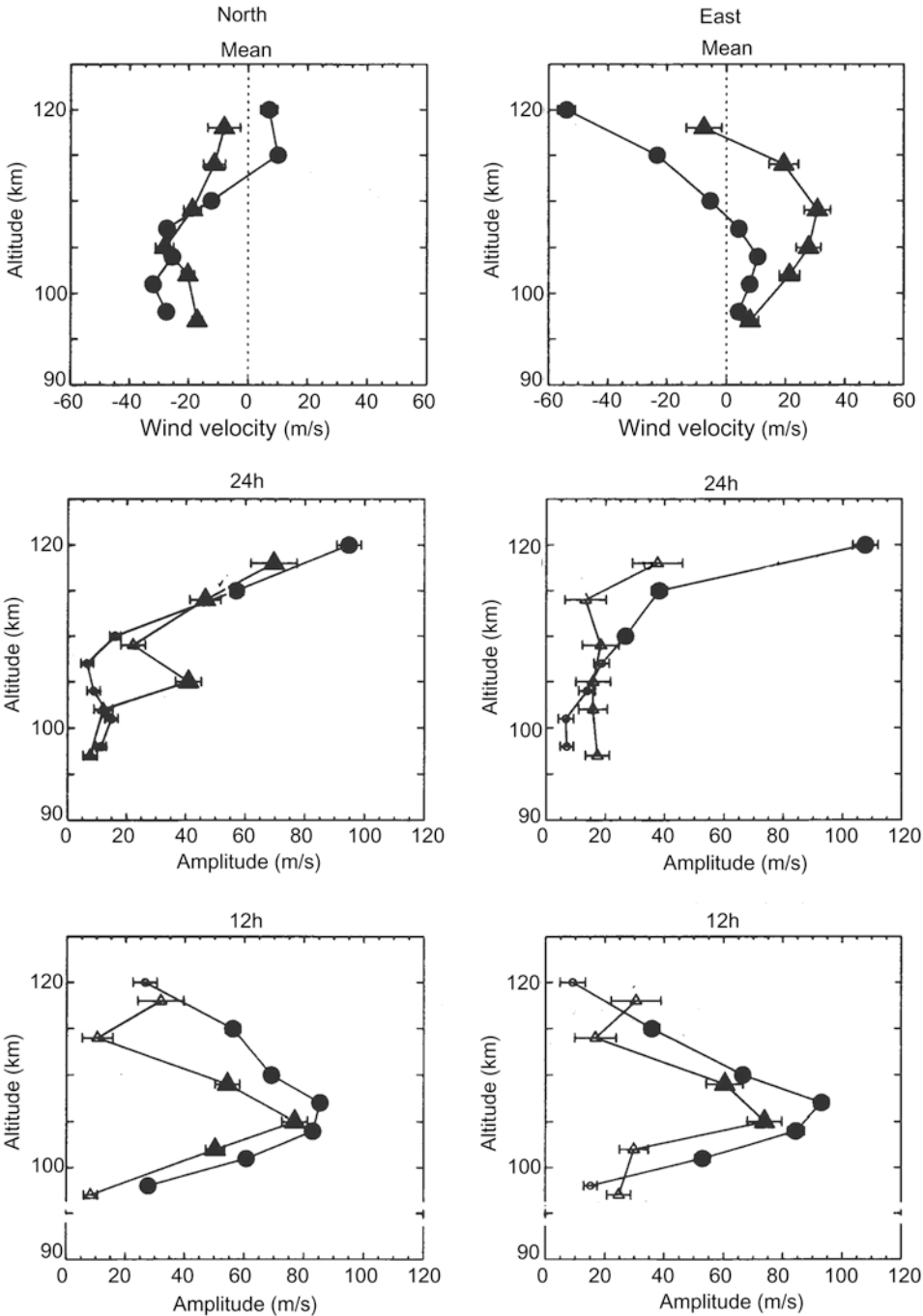


Figure 2.37. The variation with height of the northward, eastward, and downward components of the mean wind and the amplitudes of the 24-, 12-, 8-, and 6-hour tidal components. The different disturbance levels are indicated by quiet ($Ap \leq 16$) and disturbed ($Ap > 16$) conditions. The standard deviations are shown by vertical bars. (From Nozawa and Brekke, 1995.)

(a)



(b)

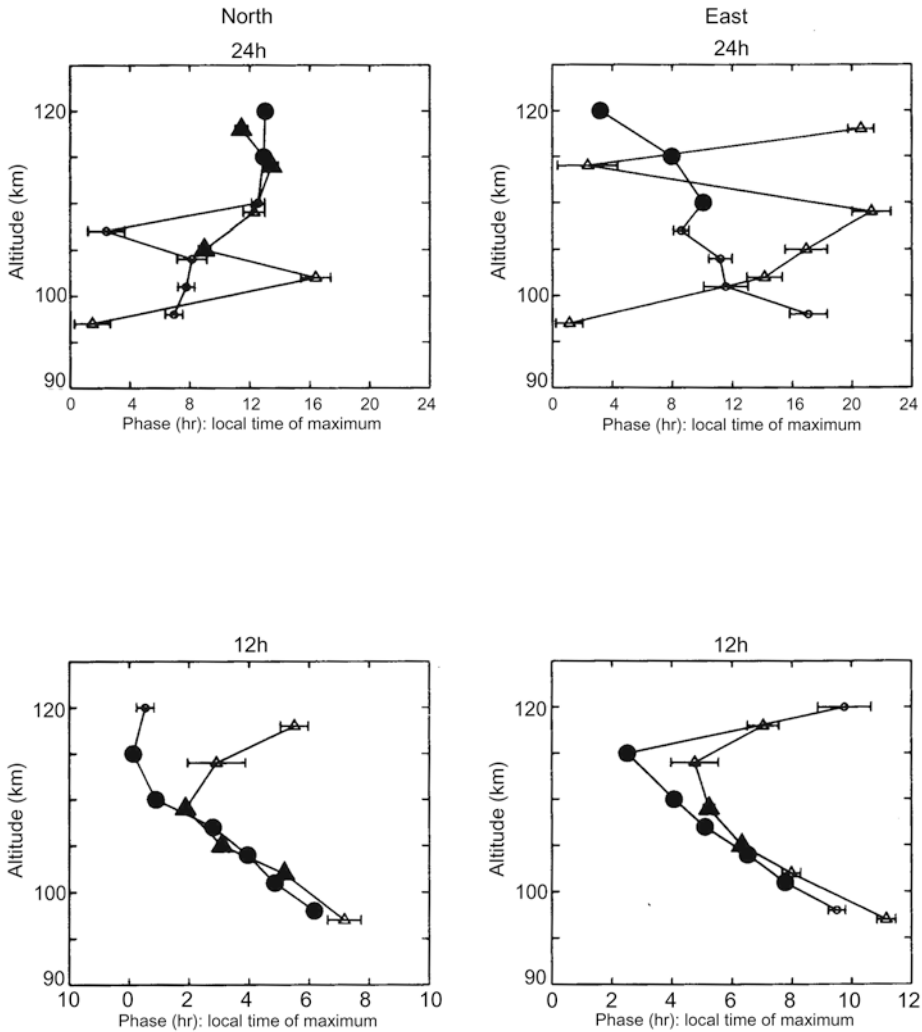


Figure 2.38. (a) Altitude profiles of mean wind (top), diurnal tidal amplitude (middle), and semidiurnal amplitude (bottom) observed at Tromsø (circle) and Longyearbyen (triangle) are presented for meridional (left) and zonal (right) components. For tidal components, larger filled symbols denote data values whose significance level is greater than 90%, smaller filled symbols whose significance level is between 90 and 50% and small open symbols denote data values whose significance level is less than 50%. Horizontal lines associated with each symbol denote error bars (1 standard deviation). (b) Corresponding phase values (in local time of maximum) are shown for diurnal (top) and semidiurnal (bottom) components for meridional (left) and zonal (right) components. (From Nozawa *et al.*, 2005.)

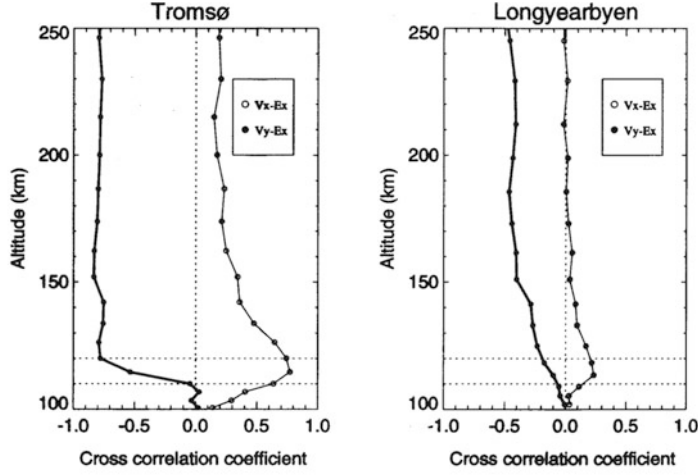


Figure 2.39. Altitude profiles of correlation coefficients between the E-region neutral wind components and the electric field as derived from Tromsø and Longyearbyen with incoherent scatter observations. (Nozawa, private communication.)

have:

$$w = \frac{H \nabla \cdot \mathbf{u}}{1 - \frac{p}{T} \frac{\partial T}{\partial p}} \quad (2.39)$$

For an isothermal atmosphere where $\partial T = 0$ we find

$$w = H \frac{\partial w}{\partial z}$$

and

$$w = w_0 \exp\left(\frac{z - z_0}{H}\right)$$

when $w = w_0$ at a reference height z_0 . Vertical velocity therefore increases with height for an expansion in an isothermal atmosphere. This comes about since density decreases by height, and in order to keep the energy flux constant the velocity must increase.

For an adiabatic expansion we get from (2.15)

$$\frac{p}{T} \frac{\partial T}{\partial p} = \frac{\gamma - 1}{\gamma}$$

and find from (2.39)

$$w = \gamma H \frac{\partial w}{\partial z}$$

and

$$w = w_0^* \exp\left(\frac{z - z_0}{\gamma H}\right)$$

Since $\gamma > 1$, the vertical velocity will increase more slowly with height in the adiabatic situation than for an expansion in an isothermal atmosphere.

The term $p\nabla \cdot \mathbf{u}$ represents a rate of mechanical work against the pressure force due to expansion or compression. We now want to relate this to the change of energy in the system.

The first law of thermodynamics per unit mass can be expressed by:

$$dq = d\varepsilon + \frac{p}{m} dV \quad (2.40)$$

where q is the heat, $d\varepsilon = c_v dT$ is the change in the internal energy, and c_v ($= 712 \text{ J K}^{-1} \text{ kg}^{-1}$) is the heat capacity per unit mass at constant volume.

From the ideal gas law we have

$$p = nkT = \rho RT$$

and since

$$\begin{aligned} \rho &= m/V \\ dV &= -m \frac{d\rho}{\rho^2} \end{aligned}$$

Inserting this into (2.40) and forming

$$\begin{aligned} \dot{q} &= \frac{dq}{dt} \\ \dot{q} &= \dot{\varepsilon} - \frac{RT}{\rho} \frac{d\rho}{dt} \end{aligned}$$

Inserting from (2.35) for $(1/\rho)(d\rho/dt)$ we have

$$\dot{q} = \dot{\varepsilon} + RT\nabla \cdot \mathbf{u}$$

And finally solving for $\nabla \cdot \mathbf{u}$

$$\nabla \cdot \mathbf{u} = \frac{1}{RT} (\dot{q} - \dot{\varepsilon})$$

and multiplying by p we finally have

$$p\nabla \cdot \mathbf{u} = \frac{p}{RT} (\dot{q} - \dot{\varepsilon}) = \rho(\dot{q} - \dot{\varepsilon})$$

The left-hand side represents the rate at which work is done by the system if the right-hand side is positive, and on the system if the right-hand side is negative. The vertical velocity can now be derived from (2.38):

$$w = \frac{\dot{q} - \dot{\varepsilon}}{g \left(1 - \frac{p}{T} \frac{\partial T}{\partial p} \right)}$$

For an adiabatic process where $\dot{q} = 0$ we now have:

$$w = -\frac{\gamma \dot{\epsilon}}{g} = -\frac{\gamma c_v}{g} \frac{dT}{dt}$$

If the internal temperature increases with time, then work must be done on the system by the surroundings and the air must contract downward. In the opposite sense, if the temperature decreases, the work is done by the system and the atmosphere expands upward. Since we have only allowed for vertical motion, this is equivalent to considering the motion of a column of air in a cylinder with a fixed base.

For external heat allowed to exchange with the system the situation can be far more dramatic, especially if \dot{q} is large. This occurs quite frequently within the auroral region of the upper atmosphere and then strong vertical motion can be expected.

2.20 EXERCISES

1. Derive the total mass of an isothermal atmosphere and compare that with the mass of the Earth.
2. Let the normalized velocity distribution in a gas in thermal equilibrium be given by:

$$f(v) = 4\pi \left(\frac{m}{2\pi kT} \right)^{3/2} v^2 \exp \left(-\frac{mv^2}{2kT} \right)$$

- (a) Derive the average speed \bar{v} .
- (b) Show that the most probable speed

$$v_{\text{m.p.}} = \left(\frac{2kT}{m} \right)^{1/2}$$

- (c) Show that the root mean square speed

$$v_{\text{r.m.s.}} = \left(\frac{3kT}{m} \right)^{1/2}$$

3. Choose a place in the atmosphere at latitude θ . In a Cartesian coordinate system x is positive eastward, y northward, and z in the vertical direction.
 - (a) Find the horizontal geostrophic wind components u and v in this coordinate system.

Let the pressure gradient around the equator look like that in [Figure 2.40](#).

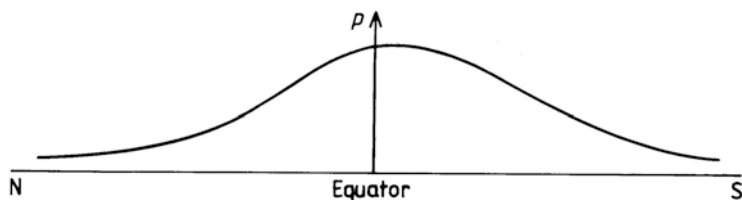


Figure 2.40

(b) Give the zonal wind directions in the northern and southern hemisphere.

(c) Does it make sense to talk about a geostrophic wind at the equator?

Let the pressure gradient around the equator look like that in [Figure 2.41](#).

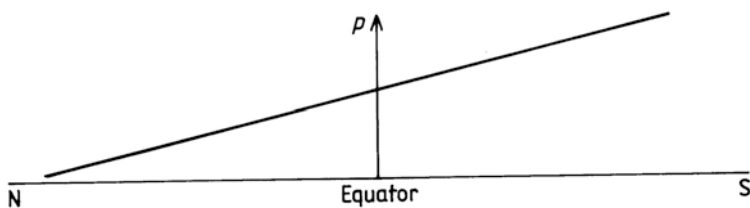


Figure 2.41

(d) What do the zonal wind directions look like in both hemispheres in this case?



<http://www.springer.com/978-3-642-27400-8>

Physics of the Upper Polar Atmosphere

Brekke, A.

2013, XXVI, 386 p., Hardcover

ISBN: 978-3-642-27400-8